NTNU

Norwegian University of
Science and Technology

Investigation of the Flow through the Runner of a Cross-Flow Turbine

Eve Cathrin Walseth

Problem Description

The objective of this thesis is to investigate the flow pattern through the runner of a cross-flow turbine. If possible, the transfer of torque during the two stages of the turbine will be measured.

A trip to Afghanistan to study the manufacturing of the cross-flow turbine is included in the thesis.

The assignment should be approached in the following manner:
1. Remodel the turbine in order to obtain necessary visibility
2. Equip the model with proper instruments
3. Visualize the flow by use of a high-speed camera
4. Evaluate the flow through the runner based on visual observations and measurements
5. A report from the trip to Afghanistan will be included in the thesis.

Assignment given: 18. January 2009
Supervisor: Torbjørn Kristian Nielsen, EPT

Norges teknisk-
naturvitenskapelige universitet
NTNU

Fakultet for ingeniørvitenskap og teknologi
Institutt for energi- og prosessteknikk

EPT-H-2009-77

MASTEROPPGAVE

for

Eve Cathrin Walseth

Våren 2009

Undersøkelse av strømning gjennom løpehjulet til en Cross Flow turbin
Investigation of the flow through the runner of a Cross Flow Turbine

Bakgrunn

I prosjektoppgaven ble det gjennomført kartlegging av virkningsgraden på en Cross Flow turbin produsert i Afganistan. Et åpent spørsmål er om strømningen gjennom løpehjulet virkelig oppfører slik produsenter av denne turbintypen hevder. Strålen treffer først skovlene øverst opp for så å strømme gjennom hjulet og treffe skovlene diametralt. I den eksisterende modellen er det vanskelig å få innsyn. Den eksisterende modellen må derfor bygges om. Ved bruk av high-speed kamera kan man da undersøke strålebanen gjennom turbinhjulet. Det skal om mulig også måles hvor stort moment man får fra strålen på henholdsvis øvre og nedre del av hjulet.

Det vil inngå i gjennomføringen å reise til Afganistan for å se på produksjonsmetodene i bedriften.

Mål
Klarlegge strømningsforholdene gjennom løpehjulet i en Cross Flow turbin

Oppgaven bearbeides ut fra følgende punkter:

1. Bygge om turbinhuset for å få nødvendig innsyn

2. Instrumentere modellen hensiktsmessig

3. Ved bruk av High-Speed kamera visualisere strømningen

4. Evaluere strømningen gjennom hjulet basert på visuell betraktning og målinger

5. I rapporten skal det inngå en reiserapport fra turen til Afganistan

Senest 14 dager etter utlevering av oppgaven skal kandidaten levere/sende instituttet en detaljert fremdrift- og evt. forsøksplan for oppgaven til evaluering og evt. diskusjon med faglig ansvarlig/ veiledere. Detaljer ved evt. utførelse av dataprogrammer skal avtales nærmere i samråd med faglig ansvarlig.

Besvarelsen redigeres mest mulig som en forskningsrapport med et sammendrag både på norsk og engelsk, konklusjon, litteraturliste, innholdsfortegnelse etc. Ved utarbeidelsen av teksten skal kandidaten legge vekt på å gjøre teksten oversiktlig og velskrevet. Med henblikk på lesning av besvarelsen er det viktig at de nødvendige henvisninger for korresponderende steder i tekst, tabeller og figurer anføres på begge steder. Ved bedømmelsen legges det stor vekt på at resultatene er grundig bearbeidet, at de oppstilles tabellarisk og/eller grafisk på en oversiktlig måte, og at de er diskutert utførlig.

Alle benyttede kilder, også muntlige opplysninger, skal oppgis på fullstendig måte. (For tidsskrifter og bøker oppgis forfatter, tittel, årgang, sidetall og evt. figurnummer.)

Det forutsettes at kandidaten tar initiativ til og holder nødvendig kontakt med faglærer og veileder(e). Kandidaten skal rette seg etter de reglementer og retningslinjer som gjelder ved alle fagmiljøer som kandidaten har kontakt med gjennom sin utførelse av oppgaven, samt etter eventuelle pålegg fra Institutt for energi- og prosessteknikk.
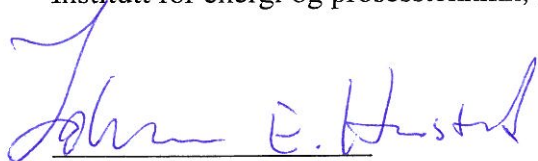
I henhold til "Utfyllende regler til studieforskriften for teknologistudiet/sivilingeniørstudiet" ved NTNU § 20, forbeholder instituttet seg retten til å benytte alle resultater i undervisnings- og forskningsformål, samt til publikasjoner.

Ett -1 komplett eksemplar av originalbesvarelsen av oppgaven skal innleveres til samme adressat som den ble utlevert fra. (Det skal medfølge et konsentrert sammendrag på maks. en maskinskrevet side med dobbel linjeavstand med forfatternavn og oppgavetittel for evt. referering i tidsskrifter).
Til Instituttet innleveres to - 2 komplette, kopier av besvarelsen. Ytterligere kopier til evt. medveiledere/oppgavegivere skal avtales med, og evt. leveres direkte til, de respektive.
Til instituttet innleveres også en komplett kopi (inkl. konsentrerte sammendrag) på CD-ROM i Word-format eller tilsvarende.

Institutt for energi og prosessteknikk, 12. januar 2009

Johan E. Hustad
Instituttleder

Torbjørn K. Nielsen
Faglærer/veileder

Medveiledere: Ole Gunnar Dahlhaug

Preface

The work presented in this thesis has been performed at The Waterpower Laboratory at The Norwegian University of Science and Technology. The thesis consists of two experimental tests performed on a cross–flow turbine manufactured by Remote HydroLight in Afghanistan. A flow visualization experiment was performed to reveal the flow pattern through the turbine, while a strain gage experiment attempted to measure the torque transferred during the two stages in the turbine. Many hours have been spent in the laboratory trying to come up with creative solutions for how to perform these experiments.

This thesis had not been possible to write if it had not been for the amazing people working in the laboratory. I would like to say a special thanks to Joar Grilstad, Halvor Haukvik and Trygve Opland for making it possible for me to perform the experiments. They put a lot of time and effort into the experimental setup. I would also like to thank my supervisor, Professor Torbjørn Kristian Nielsen, for giving me such an exciting project and sending me off to Afghanistan to study the manufacturing of the cross-flow turbine. His help through the process of writing this thesis have been invaluable.

Special thanks also go to the PhD–students Einar Kobro, Jørgen Ramdal and Pål–Tore Selbu Storli, who have been extremely helpful and creative during the process. Also, thanks to all the students at the laboratory for making it a joy to be at the university every day. This place have become like a second home to me. I also have to give a special thanks to Associate Professor Morten Kjeldsen. He became my knight in shining armor when my test results showed a higher complexity than first assumed.

Large thanks also go to Anders Austegaard and Owen Schumacher, who let me visit them in Afghanistan and sharing their knowledge of the cross–flow turbine. I would also like to give a special thank to Owens family; Debbie, Joy, Grace, Wesley and Jeremy, who welcomed me into their home and treated me like a part of their family.

Finally, I would like to thank all my friends outside of the Waterpower Laboratory and my parents, for accepting my absence from the world outside the laboratory for the past six months. They have shown a great deal of patience and supported me in any way possible.

Eve Cathrin Walseth
Trondheim, July 14, 2009

Samandrag

Ei cross–flow turbin har ein unik verkemåte fordi kraftoverføringa vert utført i to trinn. Vatn strøymer inn på løpehjulet gjennom ei rektangulær dyse og går gjennom det fyrste trinnet. Deretter går vatnet diametralt gjennom senter på løpehjulet, før det igjen møter skovlene på veg ut og gjev moment. I utviklingsland er denne turbintypen ofte nytta i småkraftverk. Turbinen har ein enkel design, som gjer den rimeleg og lett å produsere. I september 2008 vart ei cross–flow turbin produsert av Remote HydroLight i Afghanistan, installert i Vannkraftlaboratoriet ved Norges Teknisk-Naturvitenskapelige Universitet. Verknadsgradsmålingar vart gjennomført i løpet av hausten. Ein maksimal verknadsgrad på 78,6% vart oppnådd ved ei fallhøgde på 5 *meter*. Sjølv om verknadsgrada er høg, freistar det å auke denne for betre utnytting av ressursar. Eit ope spørsmål er om strøyminga gjennom løpehjulet i røynda oppfører seg slik produsentar av denne turbintypen hevdar. Det er difor av interesse å kartlegge strøyminga gjennom turbinen og å måle momentoverføringa til skovlene i dei to trinna.

To eksperiment er gjennomførde i denne oppgåva. Det fyrste eksperimentet freista å visualisere strøyminga gjennom løpehjulet ved hjelp av eit høghastigheitskamera. Dette krevde ei omfattande ombygging av turbinhuset for å sikre innsyn på løpehjulet. Høghastigheitskameraet, som var planlagt nytta i eksperimentet, vart bytta ut med eit spegelrefleks kamera og to stroboskop grunna lav kvalitet på bileta. Det andre eksperimentet freista å måle momentet på skovlene ved hjelp av strekklappar. Det var ikkje mogleg å kalibrere strekklappane innan den gjevne tidsramma for oppgåva, men ein kunne likevel oppnå eit relativt mål på momentoverføringa gjennom dei to trinna i turbinen. Verknadsgrada vart målt under begge eksperimenta, men fokuset låg på å kartlegge strøyming og momentoverføring.

Resultata frå eksperimenta viste at turbinen fungerar godt ved stor opning på dysa. Vatnet entrar då løpehjulet på eit tidleg stadium, noko som medførar at tverrstraumen vil krysse på innsida av løpehjulet, i kort avstand frå utgangen på dysa. Dette gjev gode vilkår for straumen gjennom turbina, då retninga på absolutt hastigheita vil korrespondere godt med innløpsvinkelen til blada på andretrinnet. Ved bestpunkt bidreg det andre trinnet med 53,7% av den totale momentoverføringa. Ved ei minsking i opningsgrad på dysa, vil tverrstraumen entre innsida på løpehjulet på eit seinare stadium. Dette gir ein tverrstraum med ugunstig retning inn på det andre trinnet, noko som fører til auka støt tap og lågare verknadsgrad.

Abstract

The cross–flow turbine is unique due to the generation of power during two stages. The water flows through the rectangular cross–section nozzle and enters the runner, where the first stage power is generated. The water then flows diametrically through the center of the runner, before it hits the blades on the way out, generating the second stage power. This type of turbine is often used in small hydropower plants located in less–developed countries. The turbine has a simple design, which is economical and easy to manufacture. A cross–flow turbine manufactured by Remote HydroLight in Afghanistan was installed in The Waterpower Laboratory at The Norwegian University of Science and Technology in September 2008. During the fall of 2008, efficiency measurements were performed on the turbine. A maximum efficiency of 78.6% was obtained at 5 *meter* head. However, although the efficiency is high for a turbine with such a simple design, there is a desire to improve it for better utilization of the resources. An open question is if the flow through the runner behaves like the manufacturers of this turbine type claim. It is therefore of interest to investigate the flow pattern through the runner and the distribution of torque transferred during the two stages. This is the objective of this thesis.

Two experiments are performed in this thesis. The objective of the first experiment was to visualize the flow through the runner with use of a high–speed camera. This required an extensive remodeling of the turbine in order to obtain a clear view of the flow. However, the high–speed camera had to be replaced by a single–lens reflex camera and stroboscopes, due to low quality pictures. The second experiment measured the torque transfer to the runner by the use of strain gages. The strain gages could not be calibrated within the time frame of this thesis, but a relative measure of the distribution of torque was obtained. During both experiments the efficiency was measured, but the main objective was to determine the flow pattern and torque transfer through the runner.

The results show that the turbine works well for large nozzle openings. The water enters the runner close to the nozzle outlet, leading to a cross flow entering the inside of the runner at a short distance from the nozzle. This gives good conditions for the flow, as the direction of the absolute velocity when entering the second stage corresponds well with the blade inlet angle. At best efficiency point the second stage contributes to 53.7% of the total amount of torque transferred. With decreasing nozzle opening, the cross flow enters the inside of the runner further away from the nozzle. This give a direction of the cross flow which corresponds poorly with the inlet angle of the blades at the second stage, which increases the incidence losses and gives a lower efficiency.

Contents

List of Figures

List of Tables

List of Symbols

Table 1: List of symbols used in this thesis.

Symbol	Description	Unit
a	Distance between the line of action of a force and the axis of rotation	m
C	Absolute velocity	m/s
C	Constant	$-$
E_a	Available energy	Nm/s
E_u	Utillized energy	Nm/s
e_x	Absolute uncertainty in the measurement of X	$-$
F	Forces	N
f	Filtration frequency	Hz
f_x	Relative uncertainty of the quantity X	$-$
g	Gravitational acceleration	m/s^2
H_e	Net head	m
I	Impulse	Ns
l	Length	m
δl	Change in length	m
m	Mass	kg
N	Rotational speed	rpm
n	Number of samples	rpm
P	Pressure	Pa
p	Momentum	kgm/s
Δp	Pressure difference	Pa
Q	Volumetric flow Rate	m^3/s
R	Reaction Force	N
R_1	Radius at the outer periphery of the runner	m
R_2	Radius at the inner periphery of the runner	m
S_y	Standard deviation	$-$
T	Torque	Nm
T_s	Shaft torque	Nm
t	Time	s
t	Student t factor	$-$

Table 2: List of symbols used in this thesis, continued.

Symbol	Description	Unit
U	Peripheral velocity	m/s
v_1	Velocity at turbine inlet	m/s
v_2	Velocity at turbine outlet	m/s
W	Relative velocity	m/s
X	Measured quantity	–
$\bar{Y}_\eta$	Aritmetic mean value	–
Z	Length between pressure transducer and center of the runner	m
α	Angle between absolute and peripheral velocity	rad
β	Angle between relative velocity and peripheral velocity	rad
β	Angle between the tangent of the blade and runner periphery	rad
Δt	Lenght of time interval	s
ϵ	Strain	–
η	Efficiency	%
ρ	Density of water	kg/m^3
ϕ	Speed ratio	–
ψ	Angle between the entrance and exit of the water through the runner	rad
ω	Angular velocity	rad/s

Table 3: List of prefixes, super- and sub scripts

Symbol	Description
1	Inlet first stage
2	Outlet first stage
3	Inlet second stage
4	Outlet second stage
$1 \rightarrow 2$	First stage
$3 \rightarrow 4$	Second stage
a	Available
av	Average
loc	Local
net	Net
ref	Reference
u	Utilized
u	Tangential direction
x	Direction
x	Measured quantity

Table 4: List of abbreviations used in this thesis

Abbreviation	Description
IAM	International Assistance Mission
NSP	National Solidarity Programme
SLR	Single Lence Reflex

Chapter 1

Introduction

Hydropower is an important source of renewable energy in the world today. In the industrialized nations this industry has expanded over the past decades, and the demand for knowledge and capital needed to build efficient power plants have increased rapidly. The main focus lies in utilizing the available resources as efficient as possible. However, this development has not reached the less–developed countries in the world. The main objective for these nations is to achieve a reliable source of energy in order to increase the standard of living. However, although there are available resources, the less–developed countries lack both capital and knowledge to utilize them. Therefore, a need for a more simple, but efficient, way to build a power plant is sought after.

Remote HydroLight is a company located in Afghanistan, which specializes in manufacturing small hydropower plants with funding from the U.S Core of Engineers. The company assists small villages in building and operating their own power plants. This work is an important part of the rebuilding of Afghanistan, after being at war for the past 30 years. The turbine used in Remote HydroLights projects is of the cross–flow type. The turbine design was developed under the International Assistance Mission (IAM) in 1998, and is therefore often referred to as the IAM–turbine. However, the original design has been developed further by Remote HydroLight. Labor saving features have been included to help local workshops produce a high quality turbine at a reasonable price [17].

In 2008, a cross–flow turbine manufactured by Remote HydroLight was installed at the Waterpower Laboratory at the Norwegian University of Science and Technology. Efficiency measurements were performed, and a maximum efficiency of 78.6% at 5 *meter* head was obtained [7]. This efficiency is considered high for a turbine with such a simple design. However, there is a desire to improve it in order to utilize the resources in Afghanistan even better. To be able to improve the turbine efficiency, knowledge of the flow pattern through the runner and how the torque transfer occurs during the two stages is needed. Therefore, the objective of this thesis is to reveal the flow pattern through the cross–flow turbine, and to determine the distribution of torque transferred between the two stages.

Two types of experiments are performed and reported in this thesis. The first experiment focuses on visualizing the flow through the runner. The other attempts to measure the relative amount of torque transferred to the runner by the use of strain gages. The visualization

experiment requires a remodeling of the turbine, in order to see the flow. A high–speed camera was planned used for this experiment, but for reasons explained later in this thesis, it had to be replaced with a single–lens reflex camera and stroboscopes. The strain gage experiment requires strain gages mounted on one blade, in addition to a wireless system which transmits the signal from the gages to the logging computer.

A trip to Afghanistan was included in the preparation for the two experiments performed on the cross–flow turbine. The trip resulted in a report, see appendix A, which gives an indication of the methods and limitations in production of the cross–flow turbine in Kabul.

Chapter 2

Theory

Two types of experiments are performed and reported in this thesis. The first is an experiment to visualize the flow through the runner, while the other measures the torque transferred during the two stages by the use of strain gages.

In order to execute the planned experiments and to process and analyze the data afterwards, an amount of theory related to the experiments is needed. This chapter contains the basic theory of flow through a cross–flow turbine and how to calculate the efficiency. The different types of losses in a turbine are also given. In addition theory regarding torque and experiments with strain gages is reviewed.

2.1 Flow through a cross–flow turbine

A cross–flow turbine in its simplest form consists of a runner and a nozzle. Figure 2.1 shows the manner of operation of a cross–flow turbine. The point A is defined as the nozzle outlet, B is the point where the top cover ends and F is the center of the shaft. The water flows through the rectangular cross–section nozzle and enters the runner through the nozzle entry arc. This circular arc is defined by the angle that spans out between the line that goes from A to F and the line from F to B. As the water enters through the nozzle entry arc the first stage power is generated. The water then generally crosses the inside of the runner and leaves through the lines between point C, D and E, generating the second stage power. A percentage of the water does not cross through the center of the runner, but remains entrained after entering the first stage [8].

Classification

The cross–flow turbine was originally designed as a pure impulse turbine. However, modifications to the design, making the nozzle follow the runner periphery closely have given a slight positive pressure in the gap between runner and nozzle. Haimerl [11] estimated the pressure rise in the first stage of the runner to be 6.3% of the available head for large nozzle openings. The second stage operates under constant atmospheric pressure. This has lead to the cross–flow turbine being referred to as a borderline turbine.
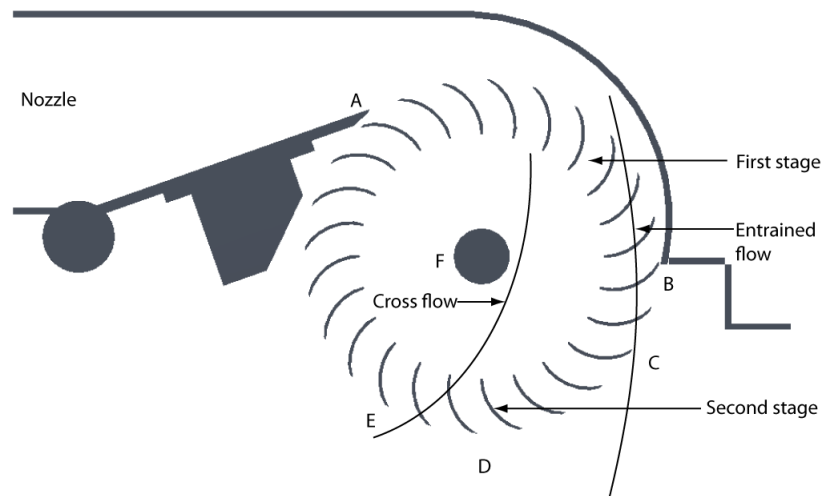
Figure 2.1: Manner of operation

Efficiency measurements performed on the IAM–turbine in 2008 [7] (see section 3.3.2), show similar characteristics. For nozzle openings larger than 80%, the flow slightly decreases with increasing rotational speed which indicates that this type of cross–flow turbine works with a small degree of reaction for openings of this size. The turbine can therefore be classified as an impulse turbine for small nozzle openings, but for larger openings the positive pressure should be taken into account.

Velocity diagrams

Velocity diagrams give an indication of the magnitude and direction of the velocity of the water. No loss through the inside of the runner is assumed, which gives equal diagrams at the outlet of the first stage and inlet of the second, see figure 2.2. In addition, an assumption of all energy extracted from the water at the turbine outlet is made, which gives no tangential component of the absolute velocity when the water leaves the runner. The velocity diagram of the entrained flow is also included in the figure, the shape of this diagram is based on Fay and Durgins findings [8] (see section 3.2 for a review of their research).

In figure 2.2 the following notations are used:

C – The absolute velocity, m/s

W – The relative velocity, m/s

U – The peripheral velocity, m/s

β – Angle between relative velocity and peripheral velocity or angle between the tangent of the blade and runner periphery, rad

$Subscript$ 1 – Water entering the first stage

$Subscript$ 2 – Water leaving the first stage

4
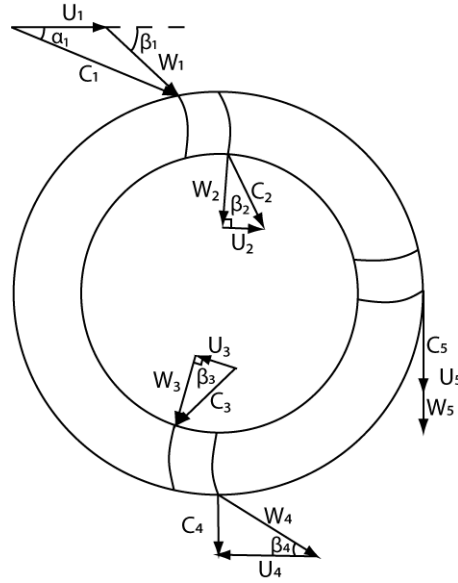
Figure 2.2: Velocity diagram

Subscript 3 – Water entering the second stage

Subscript 4 – Water leaving the runner

Subscript 5 – Entrained water leaving the runner

2.2   Efficiency

The efficiency of a turbine is defined as:

$$\eta = \frac{E_u}{E_a} = \frac{E_a - loss}{E_a}$$

(2.1)

E_u – Utilized energy

E_a – Available energy

When measuring the efficiency of a turbine in a laboratory one can measure the shaft torque, T_s, and the angular velocity, ω to enable calculation of the sum of the available energy minus the losses. When multiplying the shaft torque with the angular velocity, a direct measure of the utilized energy emerges. With these values known, the efficiency measured in the laboratory is calculated by the following equation:

$$\eta = \frac{T_s \omega}{\rho g Q H_e}$$

(2.2)

T_s – Measured shaft torque, Nm

g – Gravitational acceleration, m/s^2

Q – Volumetric flow rate, m^3/s

H_e – Net head, m

ω – Angular velocity, rad/sec

ρ – Density of water, kg/m^3

In order to use equation 2.2, shaft torque, rotational speed and flow rate needs to be measured. In addition, the pressure at the turbine inlet must be known to enable calculation of the net head, which is defined by equation 2.3. Section 4.3 explain how these units are measured in the experiments performed in this thesis.

$$H_e = \frac{v_1^2 - v_2^2}{2g} + \frac{\Delta p}{\rho g} + Z \tag{2.3}$$

v_1 – Velocity of the water at the inlet, m/s

v_2 – Velocity of the water at the outlet, m/s

Δp – Differential pressure between inlet and outlet, Pa

Z – Difference in height between pressure transducer and center of the runner, m

2.3 Losses through a turbine

According to the international standard, IEC 60193 [13], there are four types of losses in a hydraulic turbine:

- Leakage flow loss

- Specific hydraulic energy loss

- Disc friction power loss

- Bearing power loss

The standard does not directly apply to the cross–flow turbine. However, there is no literature available that explains the different losses through this turbine type. Therefore, the following review of the different types of losses that occurs in a cross–flow turbine is based on the international standard.

Leakage flow loss

Two main types of leakage occur in a cross–flow turbine. One is in the gap between the end of the top cover and the runner (point B in figure 2.1). The second is leakage between the sides of the runner and the turbine casing. The losses, according to Nielsen [15], depend on the local pressure differences in the turbine when it operates as a reaction turbine.

Specific hydraulic energy loss

The specific hydraulic energy loss contains of loss due to friction and incidence losses. The friction loss is caused by friction between the nozzle wall or the runner blades and the water. The amount of loss depends on the roughness of the surface material, and the velocity of the water. In addition, a loss in the interface between water and air is caused by friction. [7]

Incidence losses are defined as loss that occurs when the direction of the relative velocity does not correspond with the angle of the blade when entering the first and second stage. This type of losses arises when the turbine operates outside of best efficiency point. In the cross–flow turbine this type of loss will arise both in the first and second stage of the runner. Figure 2.3, shows the flow when the angle between the relative and the peripheral velocity, β, is smaller and larger than the angle between the blade and the runner periphery, β_1. This type of loss can cause separation and spreading of the flow to other blades. The loss depends on the rotational speed, angle of attack and the net head [15].

(a) $\beta < \beta_1$ (b) $\beta > \beta_1$
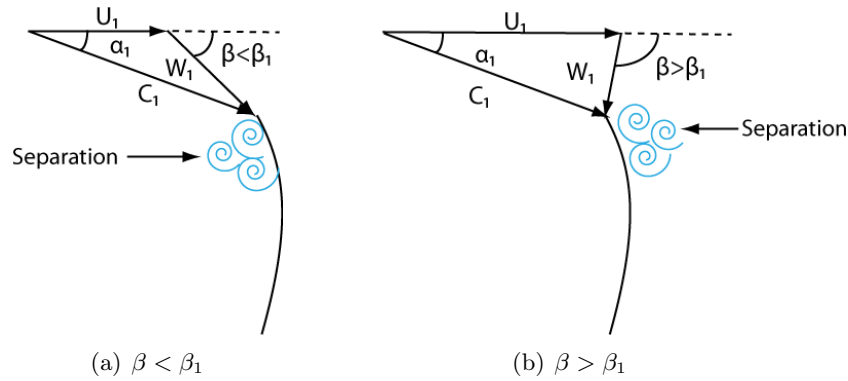
Figure 2.3: Incidence loss due to wrong inflow angle

In addition, losses can occur if the flow collides with the shaft located in the center of the runner. Remaining energy in the water at the turbine outlet is also counted for as a loss.

Disk friction loss

Disc friction loss is caused by friction from the water between rotating and stationary parts of the runner [4], and depends on the rotational speed of the runner [15]. There are two main types of disc friction losses in a cross–flow turbine. One is friction between the circular endpieces of the runner (see figure 4.1(c)) and air during rotation. The other is commonly known as windage losses, which occurs when the runner blades come in contact with saturated steam surrounding the runner blades [4]. When moving blades come in contact with inactive steam a transfer of energy from the blades to the steam occurs. This loss will have a greater magnitude when the cross–flow turbine operates as a pure impulse turbine, because the area surrounded by steam is larger.

Bearing power loss

In all turbines an amount of energy will be lost due to friction in the bearings. This loss depends on the rotational speed, and gives a direct loss in torque [15].

2.4 Torque

In this section the theory behind the experiment using a strain gage is reviewed. The strain gage is utilized to find a relative measure of the torque transferred during the first and second stage of the turbine. The magnitude of torque, T, acting on a particle is defined as [21]:

$$T = F \cdot a \tag{2.4}$$

T – Torque, Nm

F – Force acting on the particle, N

a – Perpendicular distance between the line of action of a force and the axis of rotation, m

2.4.1 Strain gage

An electrical resistance strain gage is often used when measuring the strain in structures. It is also used as a sensing element in transducers, for example in the torque flange used for the efficiency measurements performed on the turbine in this report (see section 4.3).

A strain gage measures the change in dimension of an object, called the strain, when a force is applied. With information of the strain and other parameters like property of the material, the force or torque that the strain gages is exposed to can be calculated. Figure 2.4 show a beam with a thin wire placed underneath it. The wire has a length, l, before the beam is loaded. After the force is applied, see figure 2.5, the wire has increased in length, δl, and the strain is defined as [22]:

$$\epsilon = \frac{\delta l}{l} \tag{2.5}$$

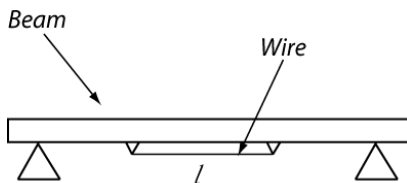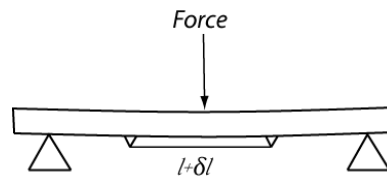Figure 2.4: Beam before load   Figure 2.5: Beam with load

The stretching of the wire will cause its electrical resistance to change, which is the same as when using a strain gage. The strain gage is a detector of strain due to change in electrical resistance. When the resulting stress of the force applied is below the material yield stress, the strains are linear functions of the applied force [22]:

$$F = C \cdot \epsilon \tag{2.6}$$

The constant, C, can be determined from analysis or calibration. With a constant length between the force, F, and the center of rotation, equation 2.4 is rewritten by combining equation 2.4 and 2.6 [22]:

$$T = C \cdot \epsilon \cdot a \tag{2.7}$$

This leads to the conclusion that the signal from the strain gage during the measurements is proportional with the strain, which is proportional to the force and torque. The use of this is shown in section 5.2.

2.4.2 Momentum theory

The strain gage can not be calibrated within the time frame of this thesis, due to its complexity. Therefore the constant, C, from equation 2.7, can not be determined. However, the goal of this experiment is to obtain a measure of the relative amount of torque transferred during the first and second stage of the turbine. Therefore, a calibration in order to determine the torque in Nm is not needed. For the processing of data, the theory of momentum and impulse is used, and therefore a review of this theory is given in the following.

The definition of momentum starts with Newton's second law for a particle of constant mass:

$$\vec{F}_{net} = m\frac{d\vec{v}}{dt} = \frac{d}{dt}(m\vec{v}) = \frac{d\vec{p}}{dt} \tag{2.8}$$

The equation states that the net force, $\vec{F}_{net}$, acting on a particle equals the time rate of change in $m\vec{v}$, which is the definition of momentum, $\vec{p}$ [23].

The change in momentum of a particle during a time interval equals the impulse of the net force that acts on the particle during that interval, $\vec{I}$ [21].

$$\vec{I} = \int_{t_1}^{t_2} \vec{F}_{net}dt \tag{2.9}$$

Figure 2.6 shows the impulse as the shaded area below the curve. An average force from the water to the blade during the time interval, Δt is defined as:

$$\vec{F}_{av} = \frac{\vec{I}}{\Delta t} \tag{2.10}$$

The average force is the constant force that gives the same impulse as the actual force in the time interval, Δt [21]. This is shown in figure 2.6 where the area of the rectangle formed by the average force, $\vec{F}_{av}$ and the time interval, Δt, equals the shaded area below the curve.

By calculating the average volt signal, by the use of equation 2.9 and 2.10 and assuming proportionality between the volt signal, force and torque, the percentage of the total amount of torque transferred during the two stages can be calculated.
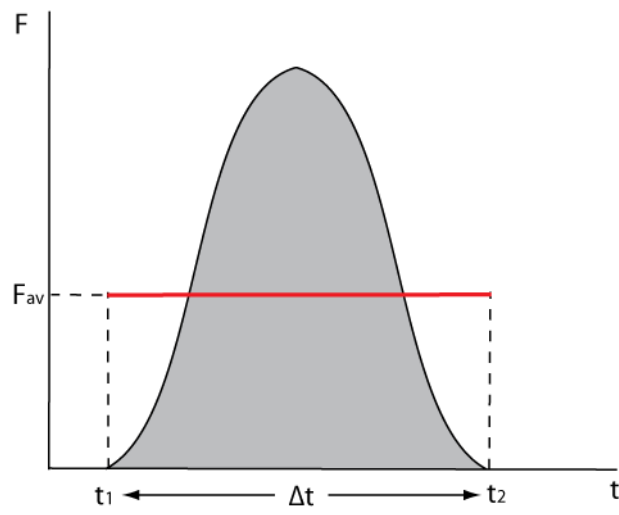
Figure 2.6: Impulse and average force

Chapter 3

Background

This chapter gives a short summary of some of the available literature on the subject cross–flow turbines. Articles which have a connection to the experiments performed in this thesis are presented in the section called previous work. In addition, a short summary of the previous experiments and analysis performed on the turbine used for these experiments is given.

3.1 Available literature

The cross–flow turbine was originally designed and patented by the Australian engineer, A.G.M Mitchell in 1903. His work was further developed by Donat Banki and presented in a series of publications between 1917 and 1919. Bankis work resulted in a theory of operation and experimental results indicating an efficiency of 80%. The popularity of the turbine increased after these publications, and it became known for its ability to be efficient at low head with a wide range of flow. Today the cross–flow turbine is mostly used in less–developed countries because the simple design makes it possible to manufacture in poorly equipped workshops.

Compared to other turbine types, the cross–flow turbine has received little attention. The main focus of the research available is to find the optimum configuration of the turbine with the use of theoretical and experimental methods.

A summary of the theoretical and experimental efficiencies achieved is given in table 3.1. The table shows that the maximum theoretical efficiency varies from 65–92%, while for the experimental studies the efficiency lies between 61–91%. These numbers are lower than for the better known turbines like Francis and Pelton. But the cross-flow turbine stands out from these types because of its ability to keep high efficiency over a wider range of flow. This characteristic makes the turbine well suited for run–of–the–river operations. The reason for the difference in theoretical efficiency lies in the assumptions made by the different researchers. The span in the experimental results can be explained by the difference in design, both of the runner and nozzle.

Thorough investigations of the design parameters affecting the efficiency have been conducted over the past century. Khosrowpanah, Albertson and Fiuzat [19] investigated the effect of the number of blades, runner diameter, and the nozzle entry arc on the efficiency with variations

Study	Year	Theoretical effciency	Experimental effciency
Banki [14]	1917-1919	92%	-
Sheperd [18]	1956	68%	-
Haimerl [11]	1960	82%	-
Mockmore and Merryfield [14]	1949	87.8%	68%
Balje [3]	1981	73%	-
		(81% with a draft tube)	-
Durgin and Fay [8]	1984	66%	61%
Khosrowpanah et al. [19]	1988	65% (assumed)	80%
Fiuzat and Akerkar [9]	1989	-	91%
Aziz and Desai [1]	1993	-	90%

Table 3.1: Theoretical and experimental efficiency

in flow rate and head. The cross–flow turbine used in these experiments was made out of clear acrylic plastic. The results concluded with the maximum efficiency increasing with an increase in nozzle entry arc (see section 2.1 for definition) from 58° up to 90°. A decrease in the efficiency was observed when the runner diameter was decreased with a constant runner width. The maximum efficiency obtained for each of the experiments occurred at the same unit speed for a constant nozzle throat–width ratio. When changing the number of blades the experiments revealed that the efficiency was strongly dependent of this parameter. At a runner diameter of 12 *inches* the optimum number of blades was 15.

Aziz and Desai [2] conducted an extensive series of experiments in order to precisely identify the favorable parameters and their impact on the cross–flow turbine performance. Their research concluded that the turbine efficiency decreases with an increase of the angle of attack at the first stage from 22° to 32°. Also an increase in efficiency was observed when the number of blades increased from 15 to 30. In addition, the ratio of inner to outer diameter of the turbine did also show an effect on the efficiency of the turbine. When increasing the ratio, the maximum efficiency showed a slight reduction. Aziz and Desai also proved that a change in the first stage blade exit angle from 90° to 55° gave a higher efficiency.

New ways to improve the turbine efficiency have also been the focus of some researchers. Fiuzat and Akerkar [9] studied the effect of interior guide tubes in the runner. The guide tubes were suppose to guide the flow between the two stages more effectively, and thereby increasing efficiency. The tests showed a 5% increase in efficiency at 70% of the rated maximum flow, increasing the efficiency up to 91%. However, when increasing the flow up to a maximum rated flow the guide tube stopped improving the efficiency due to a choking effect.

Costa Pereira et al. [16] performed an experimental study of the nozzle flow in a cross–flow turbine. Two types of nozzles was tested, one with and one without an inside guide vane. 21 pressure tappings were placed inside the nozzle to get a full overview of the pressure distribution. The results showed that the pressure distribution and efficiency was not significantly affected by the head. However, when testing both with and without a runner, the tests revealed that the pressure distribution was effected by the presence of a runner. The distribution varied significantly with the non–dimensional volume flow rate. When comparing the two nozzles tested, the one with the guide vane had the best characteristics. The nozzle

without an internal guide vane led the water poorly to the runner giving a lower efficiency.

3.2 Previous work

This section contains a review of the most relevant research performed on the cross–flow turbine with focus on the flow through the runner and the power outputs of the two stages. In addition, a short summary of the previous work performed on the IAM–turbine is given. This comprise of a theoretical analysis of the ratio of torque transfer between the two stages and efficiency measurements.

3.2.1 Flow through the cross–flow turbine

Durgin and Fay [8] performed a series of experiments with the goal of determining specific flow characteristics of a cross–flow turbine. They had a small machine constructed with a Plexiglas pressure casing and an open ended runner which allowed the flow pattern inside to be analyzed using stroboscopic and photographic techniques. The test were performed with a speed ratio, ϕ (see equation 3.1 for definition), varying from zero to one. The nozzle entry arc were also varied between 50° and 80° (see section 2.1 for definition).

$$\phi = \frac{U_1}{C_1} \tag{3.1}$$

The stroboscope revealed that a free standing jet did not exist inside the runner. The jet was instead poorly defined, and a percentage of the flow did not cross the inside of the runner but became entrained in the blades. The jet that crossed inside of the runner entered the second stage with a high degree of incidence losses, while the entrained flow was flung tangentially from the runner blades at the exit (se figure 2.2).

3.2.2 Power ratio between the two stages

The cross–flow turbine is a two stage turbine, but the effect of the second stage to the power output at the shaft is still an area with great uncertainties. A few theoretical and experimental studies have been performed, but the results differ substantially.

Theoretical studies

Table 3.2 gives a summary of the results of theoretical studies performed to determine the contribution of the first and second stage to the shaft power. The difference in the power output of the two stages is explained by the difference in assumptions made by the various researchers.

Study	Year	Power-first/second stage (%)
Mockmore and Merryfield [14]	1949	74/26
Sheperd [18]	1956	72/28
Haimerl [11]	1960	82/18
Balje [3]	1981	70/30

Table 3.2: Theoretical studies of power output

Experimental studies

Fay and Durgin [8] performed, as mentioned in section 3.2.1, a series of experiments trying to determine specific flow characteristics of a cross–flow turbine. In their experiments they attempted to measure the crossing flow by extraction, in order to determine the percentage of flow entrained in the blades. The data indicated that the second stage contributed approximately 17% to the overall performance of the turbine. However, the flow extractor used in the experiment only worked at part load. Therefore the results had to be extrapolated to obtain values for full load

The most recent experimental study was performed by Fiuzat and Akerkar [10] in 1991. Several experiments were carried out with a goal of identifying the contribution of the two stages of power generation to the shaft power. A model of the cross-flow turbine was constructed out of acrylic material at the Clemson University. The casing and the runner were constructed with an opening in the front face so that a flow diverter could be inserted to the interior of the runner. The function of the flow diverter was to intercept the crossed flow and guide it outside of the runner. This would enable the measurement of the amount of cross flow and the power generated by the first stage alone. The study concluded that the contribution of the second stage to the total power is at least 45% for a nozzle entry arc of 90°, and 41% for the 120° nozzle. However, Fiuzat and Akerkar claim that the contribution of the second stage would be higher without the presence of the flow diverter.

The results from Aziz and Akerkar are considerably different than the theoretical values calculated by earlier investigations like for instance Sheperd and Haimerl, and for the experimental results from Durgin and Fay. A reason for the difference between Durgin and Fay and Fiuzat and Akerkar could be that Fay and Durgin had to extrapolate their results to obtain values for full load. Another possible explanation is difference in runner design. The articles do not provide information about the design parameters, and therefore a comparison of the difference in design is not possible. The maximum efficiency for the cross–flow turbines used by Fay and Durgin and Fiuzat and Akerkar had an efficiency of 61% and 78%, respectively. This difference in efficiency could also have given a contribution to the varying results.

3.3 Previous work on the IAM–turbine

3.3.1 Theoretical study of torque transfer

A theoretical study of the transfer of torque between the two stages in the IAM–turbine was performed during the fall of 2008 [7]. The study was one–dimensional and assumed no losses

through the runner and no entrained flow. An expression for the ratio of torque transferred from the first and second stage was derived (see appendix C).

$$\frac{T_1 \to_2}{T_3 \to_4} = \frac{R_1^2(1 + \cos\beta_1) - R_2^2}{R_2 R_1} \tag{3.2}$$

$T_1 \to_2$ – Torque transferred during the first stage

$T_3 \to_4$ – Torque transferred during the second stage

R_1 – Radius at the outer periphery of the runner, m

R_2 – Radius at the inner periphery of the runner, m

β_1 – Angle between the tangent of the blade and runner periphery at the inlet, rad

With the known blade geometry of the IAM-turbine (see figure 4.1(d)) equation 3.2 indicated that 74% of the torque transfer occurred during the first stage, while the remaining 26% occurred during the second stage.

3.3.2 Efficiency

In 2008, a wide range of efficiency measurements were performed on the IAM-turbine, and a maximum efficiency of 78.6% was obtained [7].

The efficiency was calculated by the method described in section 2.2. A detailed description of the turbine installation in the laboratory and the instrumentation is given in section 4.2 and 4.3. Shaft torque, rotational speed, pressure at the turbine inlet and volume flow rate was measured during the tests. An overview of the instruments used, the range of the instruments and the systematic uncertainty is given in table 4.1.

The test were performed at head 5, 7 and 10 *meter*, with a rotational speed varying between 200 *rpm* and 600 *rpm*. These operating points were repeated for nozzle openings ranging from 20% and up to 100%, with an increment of 20%. The results were clear, the turbine had its best efficiency point at 5 *meter* head, with 80% nozzle opening and a rotational speed of 350 rpm. The uncertainty in this measurement was ±0.9%.

Figure 3.1 gives an overview of the results from the efficiency measured at 5 *meter* head for all five nozzle openings. Table 3.3 show the exact values of the efficiency with a rotational speed of 250, 350 and 450 *rpm*.

When analyzing the data from the efficiency measurements four trends were observed:

- The maximum efficiency increases with decreasing head.
- The efficiency increases with increasing nozzle opening for a given specific speed.
- Highest efficiency at a specific nozzle opening occurs at the same specific speed.
- For nozzle openings larger than 80% the flow rate decreases for increasing rotational speed.

Danielsen and Walseth [7] give a detailed discussion of these trends.
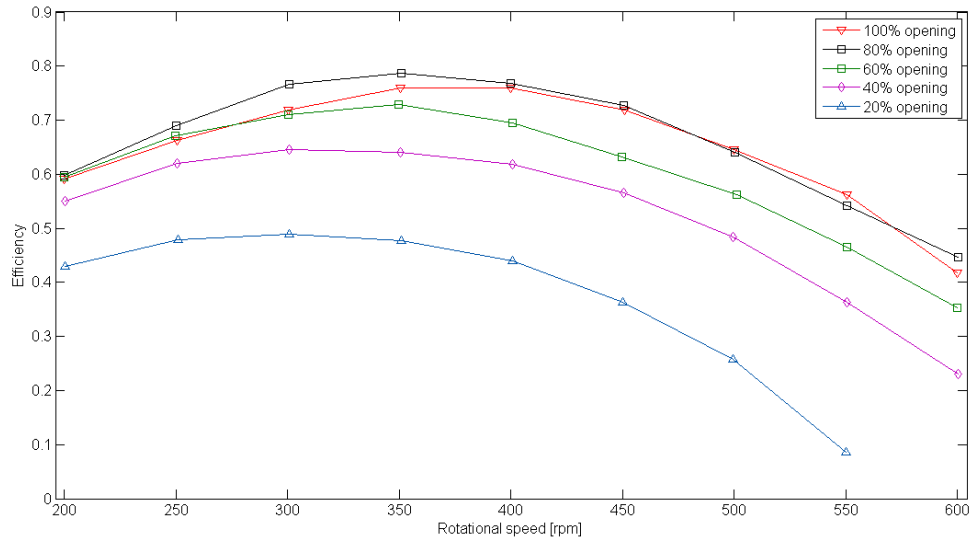
Figure 3.1: Efficiency measured at 5 *meter* head in 2008

Nozzle opening	η for 250 rpm	η for 350 rpm	η for 450 rpm
100%	66.3%	75.9%	71.8%
80%	68.9%	78.6%	72.7%
60%	67.0%	72.9%	73.9%
40%	61.9%	64.0%	56.6%
20%	47.9%	47.8%	36.4%

Table 3.3: Efficiency measured at 5 *meter* head in 2008

Chapter 4

Experimental equipment and test procedures

4.1 The IAM–turbine

A 3D–model of the cross–flow turbine used in the experiments is shown in figure 4.1(a). The turbine is often referred to as the IAM–turbine. This cross–flow turbine consists of a steel casing, an adjustable nozzle and a runner. The turbine casing is made out of steel plates which are welded together, giving a high strength. The nozzle has a rectangular shape, with an adjustable bottom plate. The wheel mounted on top of the turbine regulates the nozzle opening (see figure 4.1(b)). The nozzle entry arc on this turbine is 120° (see section 2.1 for definition). The runner consists of 24 blades symmetrically arranged between four circular plates along the plate periphery(see figure 4.1(c)). The shape of the blades, which is shown in figure 4.1(d), is circular. The blades have an inlet angle, β_1, of 30° and an outlet angle, β_2, of 90°.

For more details on the IAM-turbine design see appendix J.

4.2 Installation

The IAM–turbine was connected to a free surface loop in The Waterpower Laboratory at The Norwegian University of Science and Technology. The free surface loop, which is shown in figure 4.2, can provide a maximum of 14 $meter$ head. A pool containing 450 m^3 of water is located just below the turbine outlet (the pool is not shown in figure 4.2). A pump, in the basement of the laboratory, pumps water from the pool up to the attic and into tank 1. Tank 1 is connected to tank 2 by an open channel. Overfall pipes make sure the water level is constant. A valve located upstream the turbine is used to regulate the head in a range of $5 - 14$ $meter$. After the turbine outlet the water goes directly back into the pool.

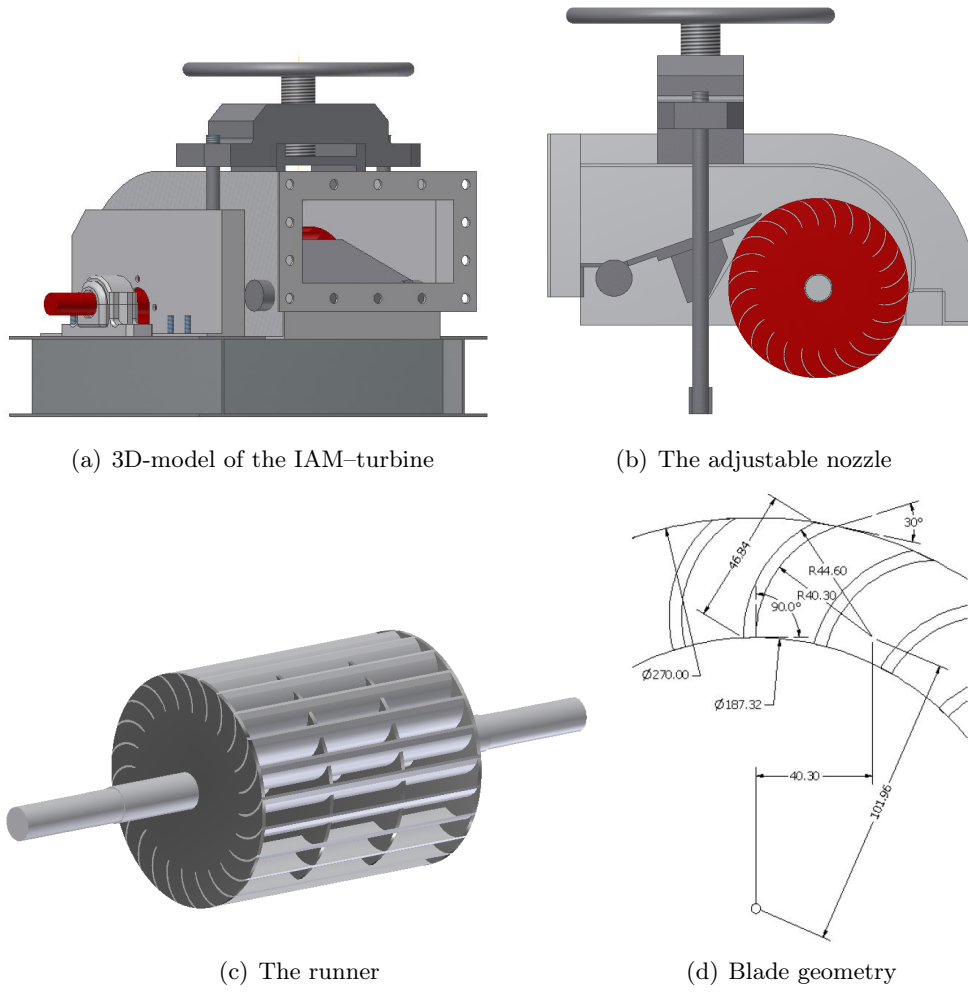Pictures of the cross–flow turbine installed in the laboratory is shown in appendix L.

(a) 3D-model of the IAM–turbine

(b) The adjustable nozzle

(c) The runner

(d) Blade geometry
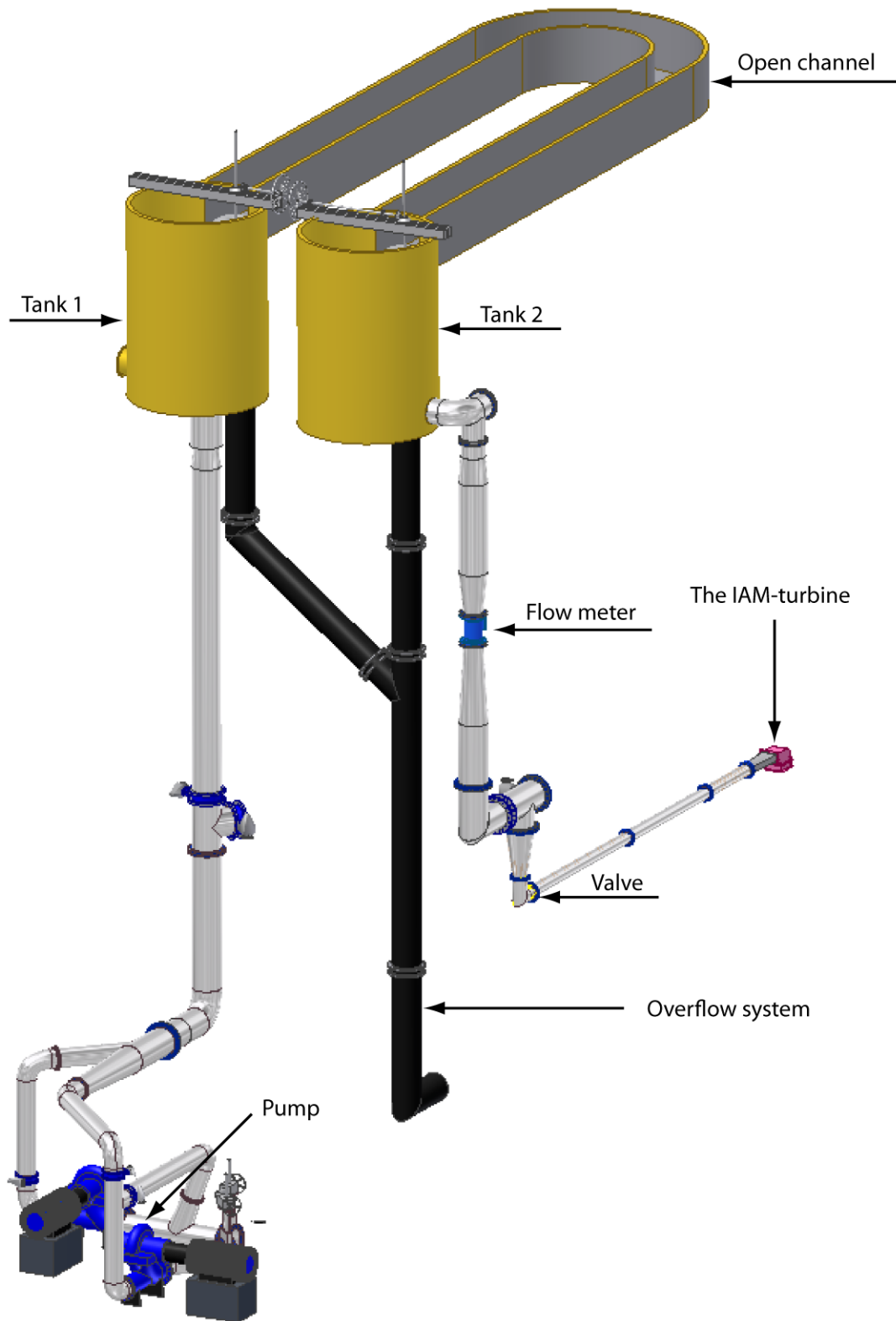
Figure 4.1: The IAM–turbine

Figure 4.2: The free surface loop

4.3   Instrumentation for measuring efficiency

The IAM–turbine was equipped with a torque flange with a built in tachometer, pressure transmitter and a flow meter in order to calculate the efficiency and other relevant parameters (see equation 2.2 and 2.3). The torque flange, of the type T10/FS produced by Hottinger Baldwin Messtechnik, measured the shaft torque and counted the revolution per minute (rpm) of the runner. The pressure was measured just in front of the turbine inlet, where four pressure taps were made. Tubes connected the pressure taps to a pressure transmitter, delivered by Fuji Electric France S.A., which measured the differential pressure between the turbine inlet and the atmospheric pressure. An electromagnetic flow meter, of the type Krohne IF4000, was connected to the pipe which goes from tank 2 in the attic down to the turbine (see figure 4.2). The range and systematic uncertainties of the instruments is shown in table 4.1. All the instruments were calibrated in October/November 2008 [7].

Quantity	*Device*	*Range*	*Uncertainty*
Torque at turbine shaft	Torque flange	$\pm1000\ Nm$	$\pm0.11\%$
Pressure at turbine inlet	Pressure transmitter	$\pm2000\ kPa$	$\pm0.30\%$
Flow rate into the turbine	Electromagnetic flow meter	$0 - 1\ m^3/s$	$\pm0.15\%$
Rotational speed	Tachometer	$0 - 12000\ rpm$	$\pm0.71\%$

Table 4.1: Measuring devices

A program made in LabView (see appendix F), was used to log data during the experiments. The program collects signals from the measuring instruments and calculates the efficiency and other relevant parameters.

4.3.1   Test procedure for efficiency measurements

The efficiency was measured during the flow visualization and the strain gage experiments. For each speed and nozzle opening tested, the LabView program took three samples measuring shaft torque, rotational speed, inlet pressure and flow rate. The efficiency was calculated for each sample. An uncertainty analysis of the measured efficiency was executed and can be viewed in appendix B.

4.4   Flow visualization

4.4.1   Remodeling

Documentation of flow through a turbine with use of a camera was only possible with an unobstructed view to the flow and considerable amounts of light. The IAM–turbine has, as shown in figure 4.3, a closed design. The casing and the circular endplates in the runner makes flow visualization impossible without modifications to the original design. The changes to the turbine design were decided in cooperation with experienced mechanics in The Waterpower Laboratory. The main focus was to ensure full access to the flow without compromising the

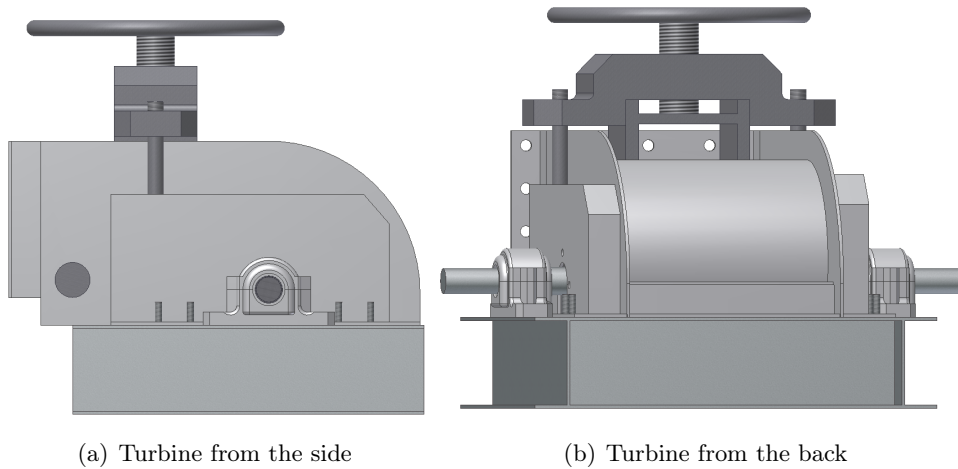(a) Turbine from the side   (b) Turbine from the back

Figure 4.3: Turbine before remodeling

strength of the turbine. The turbine had to endure a pressure of 5 *meter* head as a minimum, in order to perform tests at best efficiency point (see section 3.3.2).

The demands for flow visualization were met by removing a large piece of the left sidewall giving a direct view into the runner. The circular endpiece of the runner facing left was cut off, and replaced with a plate of Plexiglas. The plate had milled out traces to fit the blades, and was connected to the blades with an adhesive for Plexiglas called Thensol 70. The changes made to the sidewall and runner is shown in figure 4.4(a). In addition to the changes made on the sidewall, the bearing holder on the left side was replaced with a smaller one and a piece of the frame was replaced with Plexiglas to get a view of the lower part of the runner.

(a) Turbine from the side   (b) Turbine from the back
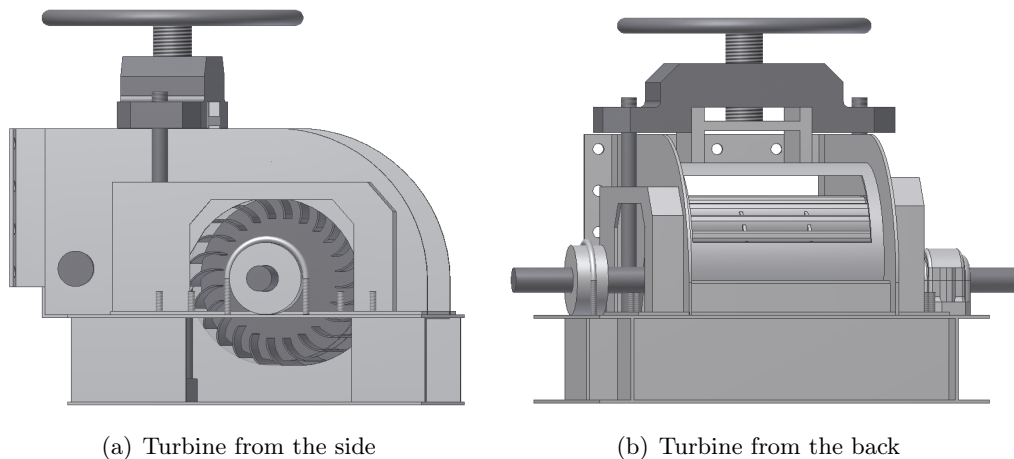
Figure 4.4: Turbine after remodeling

To ensure good quality of the pictures from the camera, the lighting must be sufficient. The original design of the turbine casing did not let in enough light, not even with the changes made to the left side. Therefore a part of the top cover above the runner was cut off and replaced with Plexiglas. The width of the removed part was decided based on the need of a so called "workers edge". The purpose of the edge was to keep the strength of the casing

as intact as possible. The mechanics estimated that 15 *mm* on each side would be sufficient. Figure 4.4(b) shows the back of the turbine casing after the changes were made.

A slight decrease in efficiency from the experiments conducted the fall of 2008 [7] (see section 3.3.2), is expected due to the remodeling of the turbine.

4.4.2   Camera

Initially a high–speed camera was planned used to document the flow through the runner. Unfortunately the camera was not able to capture the entire flow through the runner; it could only capture a couple of blades at the time. In addition the quality of the pictures was low. A single-lens reflex (SLR) camera and two stroboscopes were therefore used instead. The SLR camera was of the type Canon EOS 50D, and could take 6.2 pictures per second. Combined with the effect of the stroboscopes, it was possible to get a picture of the flow through the runner. The camera had to be placed in three different positions to get a full overview of the flow. Three racks were made for the camera, one with a view of the upper part of the runner, one for the lower part and one with a full view of the runner.

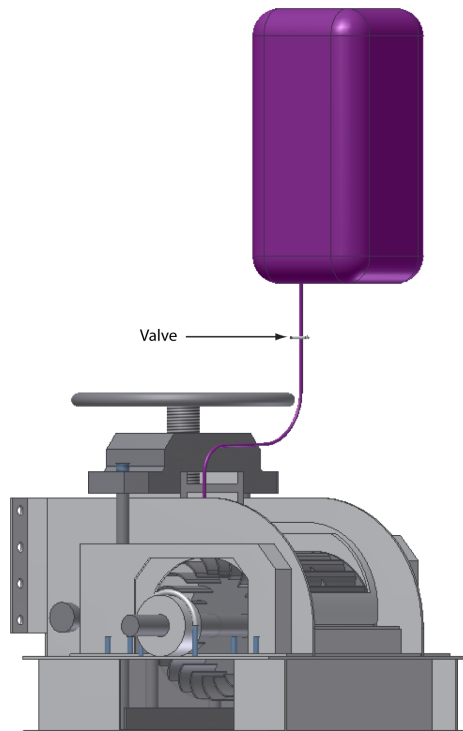### 4.4.3   Injection system

Figure 4.5: The injection system

The use of color or reflecting particles in the water can simplify the observation of flow through a runner. Potassium permanganate is a substance which becomes purple in contact with

water. The substance is most often used as an antiseptic agent, but due to its intensive color when mixed with water, it is suitable for visualizing flow through the turbine. A small hole was drilled in the turbine casing, and an injection pipe was connected to this hole. The pipe was placed just above the runner right after the nozzle exit. The injection system consisted of a large can filled with potassium permanganate mixed with water, which was placed approximately 0.7 *meter* above the turbine (see figure 4.5). A plastic tube connected the tank with the injection pipe, and a valve placed in between regulated the flow of color.

4.4.4   Test procedure for flow visualization

The tests are performed with a constant head of 5 *meter*, and nozzle openings ranging from 20% to 100%, with an increment of 20%. For each opening the rotational speed varied between 250 *rpm* and 450 *rpm*. These values were decided based on previous tests showing that the best efficiency point for 5 meter head occurs with a rotational speed of approximately 350 *rpm* [7]. For each point of operation the camera was placed in three different positions and pictures in each position was taken both with and without color and stroboscopic effects.

4.5   Torque transfer

Measuring the torque transferred from the water to the blades in Nm was a complex problem, both with placement of the strain gage and processing data. The time frame of this report does not allow this type of problem. However, a relative measure of the torque transfer can be performed. In order to measure the relative torque transfer during the first and second stage of the runner, two strain gages was placed on a blade; one gage on the suction side of the blade, the other on the pressure side. However, during the flow visualization experiments the strain gage on the pressure side of the blade was torn off. This led to a reopening of the turbine casing, by removing the Plexiglas plate on the top cover. The loose strain gage was removed, and more adhesive was put on the strain gage on the suction side to ensure that it would stick. The loss of one strain gage did not change the planned tests, because one gage is enough to obtain a relative measure of the torque transferred.

For these experiments a strain gage with a nominal resistance of 350 Ω was used. When remodeling the turbine, one side of the runner was replaced with Plexiglas, as mentioned above. To ensure that the strain in the blade would be large enough to receive a good signal from the strain gage, one blade was slightly looser connected to the endpiece of Plexiglas than the others. The milled out trace in the plate was larger for this blade than the others, and silicon was used to glue them together. The signal from the strain gage was sent by wire to a wireless transmitter placed on the end of the shaft. The transmitter, of the type Wireless Link Digital Telemetry System, sends the signal to a receiver connected to the logging computer.

A program made in LabView, see appendix G, was used to log the data from the receiver with a sample rate of 4000 samples per second.

4.5.1   Test procedure for measuring torque transfer

All tests are conducted with a net head of 5 meter. The tests are performed for nozzle openings ranging from 20% up to 100%, with an increment of 20%. For every nozzle opening the rotational speeds of 250 *rpm* and 350 *rpm* are tested. Due to concerns about the bearings condition it was decided not to test at a higher rotational speed. In order to ensure that the data is correct, the tests are performed three times at each operating point.

Chapter 5

Data processing

After an extensive search for literature on flow visualization and strain gage experiments performed on a cross-flow turbine, it can be concluded that the experiments in this report were the first to be performed on this turbine type. One article on flow visualization was found, and is reviewed in section 3.2.1. However, this article does not attempt to draw the general flow patterns through the runner. When it comes to the strain gage measurements no articles were found that is directly related to this experiment. It can therefore be concluded that a common procedure for how to process the data from the two experiments conducted does not exist.

In order to determine how to process the data retrieved from the flow visualization and the strain gage measurements, PhD–students, associate professors and professors within the field of hydropower was consulted. The data from the strain gage measurements were more complex than assumed before the tests were conducted. The signal contained an amount of noise, in addition to large variations for different nozzle openings. In order to find a standard procedure for analyzing the data at different nozzle openings, several programs were made. In the end, what gave the most consistent treatment of data was a combination of a program made in Matlab and one in LabView. In addition, the signal from the 20% opening had to be excluded.

The following text gives a review of how the data from the two experiments were processed.

5.1 Flow visualization

The data collected from the flow visualization experiments consists of pictures taken with a SLR camera and observations. In addition to this, signals from the measuring equipment were logged, giving shaft torque, inlet pressure, flow rate and rotational speed. These data were used to calculate the efficiency of the turbine. Formulas used for these calculations are reviewed in section 2.2.

The data from the pictures and observation was examined and compared, resulting in drawings of the flow through the runner at different nozzle openings and rotational speed. The data is not accurate, but gives a good indication of the flow pattern through the runner.

Example of pictures taken during the flow visualization experiments is shown in appendix K.

5.2   Torque transfer

The original signal from the strain gage measurements was first plotted in order to see the shape. At large openings the signal confirms that torque transfer occurs during two stages in the runner. The plot of the original signal, shown with blue in figure 5.1, shows two peaks of different sizes. The signal repeats itself during the time frame of the plot. However, the signal contained an amount of noise, which needed to be filtrated before further use. In the following text the large peak is also referred to as peak 1 or first peak, while the small peak is referred to as peak 2 or second peak.
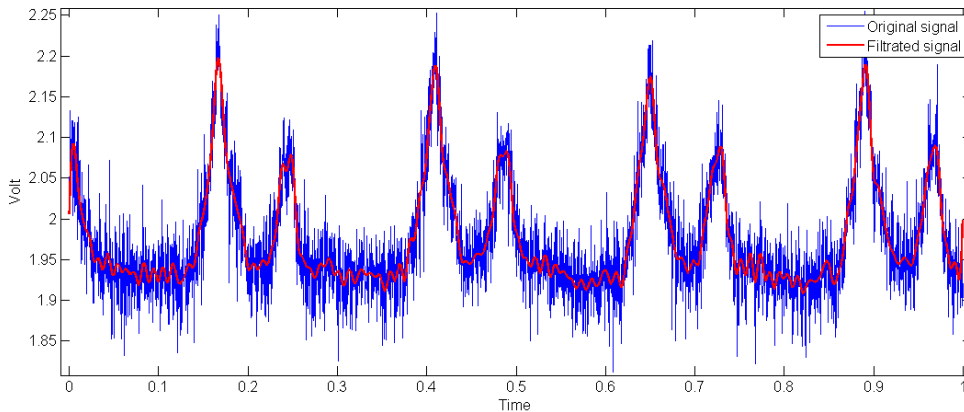

Figure 5.1: Original and filtrated signal for 80% nozzle opening at 250 *rpm*

A low pass filter in LabView was used on the signal. Different filtration frequencies were tested, with the purpose of finding one that gave smooth curves without losing the shape of the original signal. A frequency of 100 Hz was decided most suitable, plotted as red in figure 5.1. It remained close to the original data, but was still smooth enough to seek out the start and end point of the peaks. However, the signal for 20% nozzle opening contained a considerable amount of noise with this filtration frequency. In order to get curves smooth enough for further analysis, this signal had to be filtered with a frequency of 30 Hz. This caused the original signal to lose its shape. Therefore the 20% opening will be excluded from the standard data processing and analyzed separately.

Calibration of the strain gage was not possible at the time of the experiments. Therefore, the signals lack a common zero point reference for use when calculating the torque transferred. However, a relative measure of the torque can be found by integration of the area below the curves. The theory behind the integration is shown in section 2.4.

After filtration of the signal, the integration can be performed by the use of two programs. A program made in Matlab (see appendix I) plots the filtrated strain gage signal versus the time. From the plot the user manually picks out the start and end points of the peaks, by use of the Data Cursor Tool. For the tests performed at 250 *rpm*, four peaks of each size were identified, and five peaks for 350 *rpm*. The length in time for each peak and the length between the start of the large peak and the start of the small peak, are calculated. In addition the program returns the average value for these lengths.

Associate Professor Morten Kjeldsen made a program in LabView (see appendix H) which integrates the area under the two peaks with a few input data:

- The average length of peak 1 and peak 2 (from Matlab)

- The average length between the start of peak 1 and the start of peak 2 (from Matlab).

- Peak and valley threshold values

Figure 5.2 shows the values used for the LabView integration. t_1-t_2 defines the length of the large peak, while t_3-t_4 defines the small peak. The value of t_1-t_3 gives the location of the second peak. Threshold values define the location of the peaks and valleys for integration and the lengths define the integral time. The program calculates a zero point reference, 0_{ref}, for the signal. In addition a local zero point, 0_{loc}, is defined as the volt value at the starting point of the integration of the largest peaks. The integration is first performed between the curve of the peaks and the zero point reference. Afterwards, the area between the local zero point, 0_{loc}, and the zero point reference, 0_{ref}, is subtracted. This gives the area under the peaks, shaded with grey in figure 5.2.
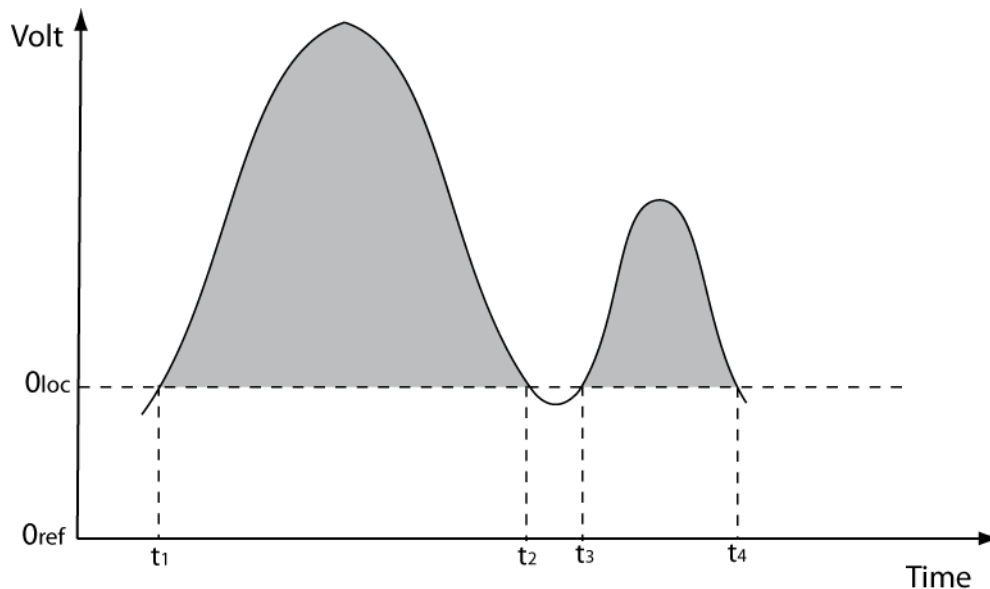

Figure 5.2: Integration in LabView

The values calculated in Matlab and LabView will be further processed in a spreadsheet calculating the amount of transferred torque during the two stages in percent. In addition the angle between the water entering the first stage and leaving the second, ψ (see figure 5.3), is calculated.

5.2.1   Processing data for 20% nozzle opening

The 20% nozzle opening had to be analyzed separately from the other openings, due to the large amount of noise in the signal. The method of processing the data were the same as for the larger openings, but the signal had to be filtrated with a frequency of 30 Hz. This gave
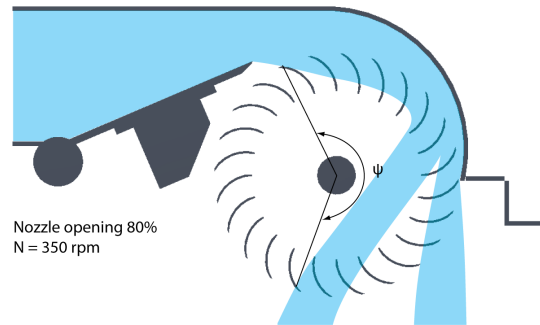
Figure 5.3: Definition of angle, ψ, between water entering and leaving the runner.
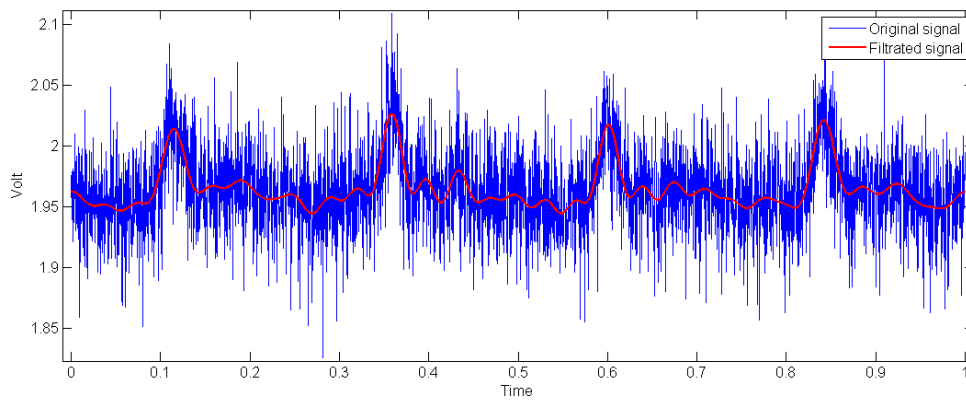
Figure 5.4: Original and filtrated signal for 20% opening at 250 rpm

a smooth curve for further processing. However, by filtrating the signal at a lower frequency the original signal lost some of its shape (see figure 5.4), and therefore important information might have been filtrated out. The results that emerge from this analysis still gives a good indication of the torque transfer during the two stages, but one should keep in mind that the filtration might have caused loss of important information.

Chapter 6

Results

This chapter contains a review of the results from the two experiments performed in this thesis. A discussion of these results is given in chapter 7.

6.1 Flow visualization

General flow pattern

After processing the data from the flow visualization experiments, the general flow patterns through the turbine for different nozzle openings was drawn. The flow pattern through the turbine for all five nozzle openings at a rotational speed of 350 rpm is shown in figure 6.2 This speed is chosen based on the efficiency measurements that were performed during the experiments. The results showed that all nozzle openings, except at 60%, had their best efficiency at this rotational speed. Figure 6.1 presents an overview of the efficiency measured for each rotational speed and nozzle opening tested. Table 6.1 show the exact values. An uncertainty analysis of these results is executed in appendix B. The uncertainties are given as parenthesized values in table 6.1.

Nozzle opening	η at 250 rpm	η at 350 rpm	η at 450 rpm
100%	69.3% (±1.05%)	77.5% (±1.96%)	70.6% (±2.87%)
80%	70.5% (±1.86%)	76.8% (±0.87%)	67.3% (±3.29%)
60%	61.7% (±1.68%)	60.2% (±0.95%)	44.8% (±1.43%)
40%	61.6% (±1.37%)	64.7% (±2.83%)	55.1% (±2.84%)
20%	53.7% (±1.37%)	54.9% (±2.85%)	45.1% (±3.43%)

Table 6.1: Efficiency measured during the flow visualization experiment. The uncertainties are given as parenthesized values.

When comparing figure 6.2(a) to 6.2(e) one can observe that the point where the blades starts filling with water changes with the nozzle opening. An increase in nozzle opening leads to a filling of the blades closer to the nozzle outlet. Change in the point where the water enters the blades results in a change in entry point for the cross flow inside the runner. When the blades
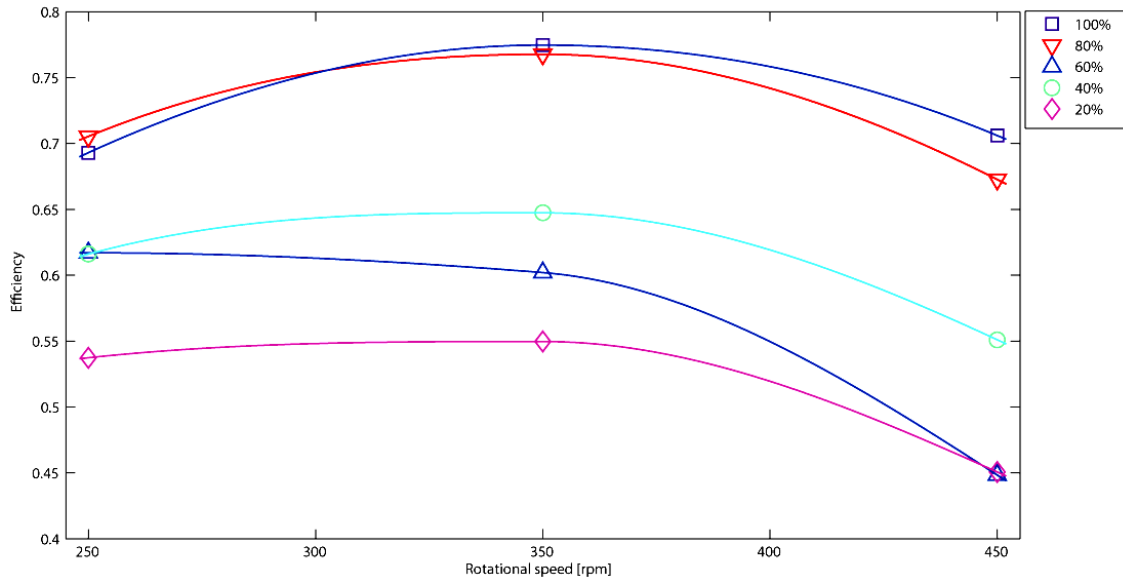
Figure 6.1: Efficiency measured during the flow visualization experiments.

starts filling up close to the nozzle outlet, the cross flow enters the inside of the runner at an earlier stage. This characteristic was most visible at 80% and 100% opening, where the inside jet went almost vertical through the center of the runner (see figure 6.2(a) and 6.2(b)). The opposite was observed at 20% nozzle opening. The cross flow entered the inside of the runner close to the outlet, and crossed nearly horizontal through (see figure 6.2(e)). The efficiency measurements performed during the experiments indicates that the efficiency decreases with decreasing nozzle openings (see figure 6.1).

At every nozzle opening a certain amount of water was entrained in the runner and flung almost tangentially out at the turbine outlet. Together with this flow, two leakage flows were observed. One in the clearance between the runner and the top cover, the other occurred on the sides between the runner and the turbine casing. The leakage on the sides was observed to increase with increasing nozzle opening. However, according to table 6.1, the efficiency did not decrease with the leakage. The total amount of leakage and entrained flow could not be measured at this point due to the experimental setup.

The direction of the absolute velocity at the runner outlet varied with nozzle opening. At large openings the absolute velocity changed direction through the second stage, see figure 6.3. The variation in direction faded out with decreasing nozzle openings, and the direction of the absolute velocity remained almost constant through the second stage. This is best observed at 20% opening, see figure 6.4.

Change in pattern with change in rotational speed

The tests were performed at three different rotational speeds for each nozzle opening. A tapering of the cross flow inside the runner was observed when the rotational speed increased, see figure 6.5. At 20% opening at 450 *rpm* the jet inside the runner was almost nonexistent,

Nozzle opening 100%
N = 350 rpm

Cross flow

Entrained flow

Leakage flow

(a)

Nozzle opening 80%
N = 350 rpm

Cross flow

Entrained flow

Leakage flow

(b)

Nozzle opening 60%
N = 350 rpm

Cross flow

Entrained flow

Leakage flow

(c)

Nozzle opening 40%
N = 350 rpm

Cross flow

Entrained flow

Leakage flow

(d)

Nozzle opening 20%
N = 350 rpm

Cross flow

Entrained flow
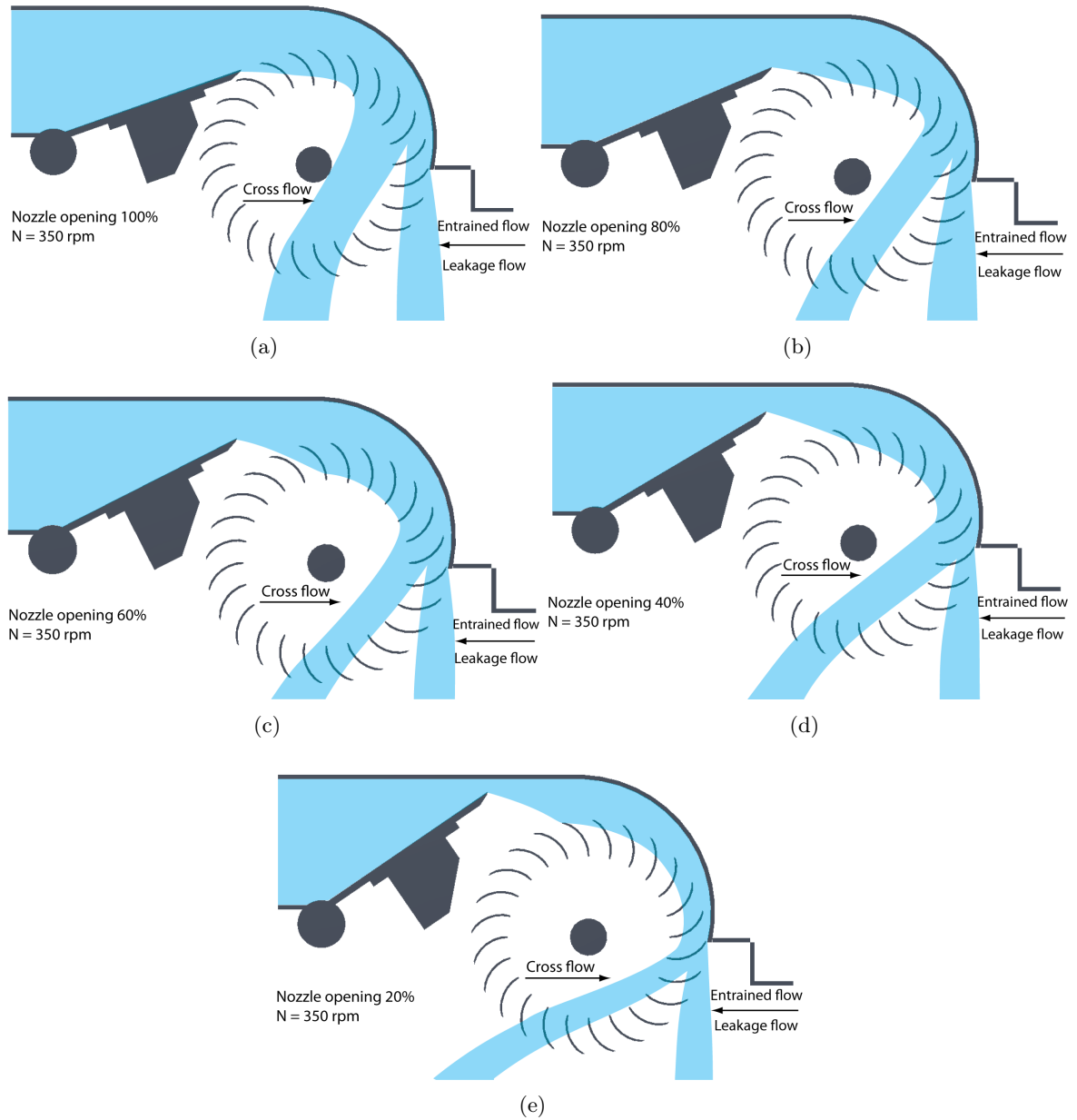
Leakage flow

(e)

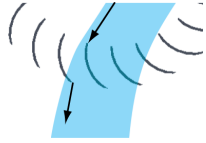Figure 6.2: General flow patter at 350 rpm
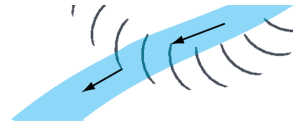
Figure 6.3: 100% opening at 350 *rpm*   Figure 6.4: 20% opening at 350 *rpm*

and a large percentage of water became entrained in the runner. A reduction of the efficiency by 10 percentage points was measured when going from 350 *rpm* to 450 *rpm*. The change was approximately equal for all five nozzle openings (see table 6.1). The amount of entrained flow increased with increasing rotational speed for all nozzle openings. However, when increasing the rotational speed from 250 *rpm* to 350 *rpm* the efficiency enhanced for every opening except at 60%.
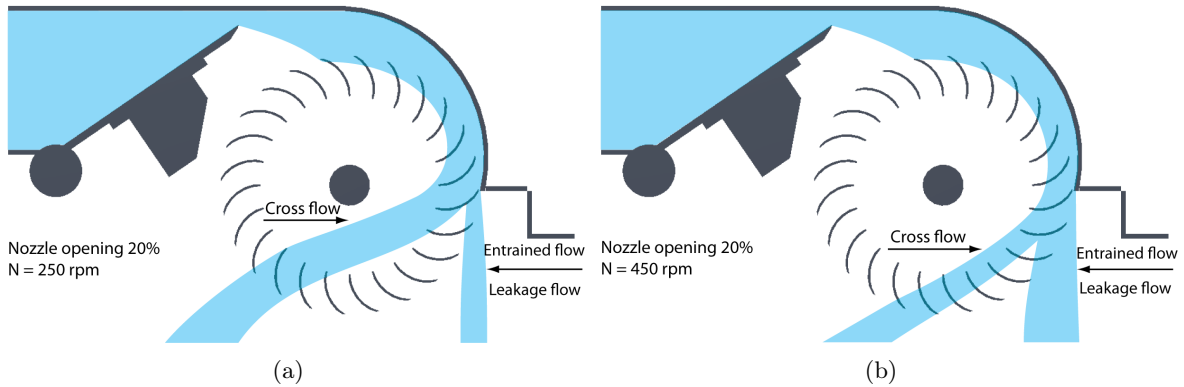

Figure 6.5: Tapering of jet when increasing the rotational speed

As for change in nozzle opening, the change in direction of the absolute velocity through the second stage was observed to vary with the rotational speed. When the rotational speed increased, the change in direction between inlet and outlet at the second stage decreased. At 450 *rpm* the change in direction of the absolute velocity was close to zero.

When changing the rotational speed from 350 *rpm* to 250 *rpm* a decrease in efficiency of 6.3 percentage points at 80% nozzle opening and 8.1 percentage points for 100% opening was observed. The corresponding drop for 40% and 20% openings was measured to 1.2 and 3.1 percentage points, respectively. Observation of the flow at 80% and 100% opening revealed a collision with the shaft at low rotational speed, see figure 6.6. The collision was most visible at full opening. Figure 6.6(b) shows that a part of the water went over the shaft after the collision and left the turbine just below the nozzle.
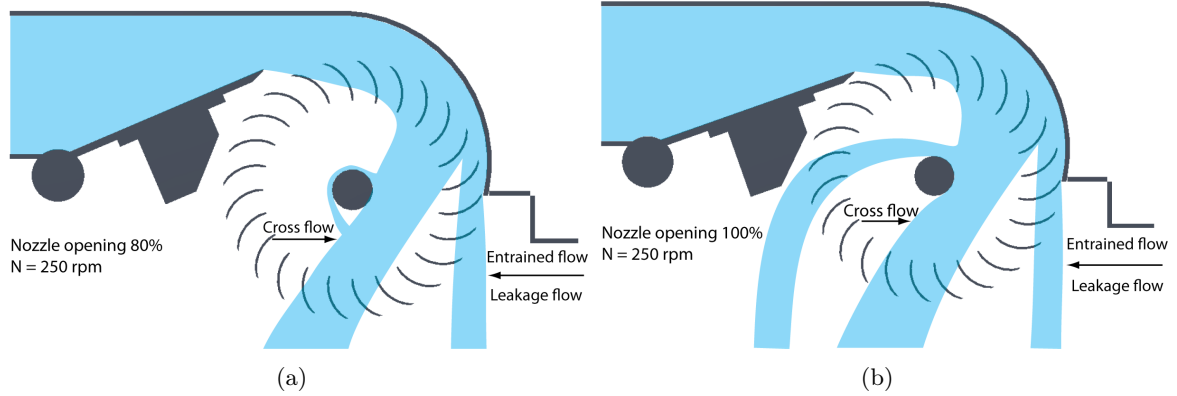
Figure 6.6: Collision with shaft at 250 *rpm*

6.2 Torque transfer

Ditribution of torque

The main results from the processing of the strain gage signal are presented in table 6.2. A graphical presentation is given in appendix E. The table show how the total amount of torque transferred is distributed over the first and second stage in the runner. In addition, the table shows the value of the angle, ψ, which is the angle that spans out between the entrance and exit of the water through the runner (see figure 5.3).

	250 *rpm*			350 *rpm*		
Nozzle opening	*First stage*	*Second stage*	ψ	*First stage*	*Second stage*	ψ
100%	49.4%	50.6%	238°	46.3%	53.7%	241°
80%	58.2%	41.8%	201°	57.2%	42.8%	181°
60%	60.5%	39.5%	185°	57.7%	42.3%	176°
40%	63.6%	36.4%	193°	60.8%	39.2%	167°

Table 6.2: Distribution of torque

A new set of efficiency measurements were performed during the strain gage measurements, revealing that the efficiency had decreased between the experiments. In addition, the measurements revealed a significant variance in the results from the flow visualization and strain gage experiments for the efficiency at 60% nozzle opening. Table 6.3 shows the efficiency obtained from the strain gage experiments. When looking at all nozzle openings, except 60%, there is a decrease in efficiency from the flow visualization experiments. An uncertainty analysis of these results is executed in appendix B. The uncertainties are given as parenthesized values in table 6.3.

Trends in distribution of torque

A general trend in the distribution of torque transfer can be observed in table 6.2. With an increase in opening, the distribution between the first and second stage show a tendency

Nozzle opening	η at 250 rpm	η at 350 rpm
100%	67.6% (±0.86%)	75.3% (±0.86%)
80%	67.4% (±2.56%)	73.4% (±1.10%)
60%	63.7% (±2.77%)	66.9% (±1.83%)
40%	56.2% (±3.87%)	58.9% (±2.47%)
20%	43.8% (±3.57%)	46.0% (±1.06%)

Table 6.3: Efficiency measured during the strain gage experiment. The uncertainties are given as parenthesized values.

to level out. At 100% opening with a rotational speed of 250 *rpm* the contribution of the first and second stage of the total transferred torque is 49.4% and 50.6%, respectively. When decreasing the nozzle opening, the first stage starts to contribute more to the total transfer of torque. This can be seen for a 40% opening in table 6.2. The first stage contributes here to 63.6% of the transferred torque, which is an increase of 14.2 percentage points compared to a nozzle opening of 100%. The efficiency also shows a variation between these two nozzle openings, while the 100% opening at 250 *rpm* have an efficiency of 67.6%, the efficiency is only 56.3% for 40% opening.

Table 6.2 shows the change in distribution with increasing rotational speed. At a rotational speed of 350 *rpm*, the second stage contributes approximately 3 percentage points more than at 250 *rpm* for all nozzle openings, except at 80%. It should also be noted that all nozzle openings showed an increase in efficiency for the same change in rotational speed (see table 6.3). The distribution of torque at a rotational speed of 350 *rpm* with a nozzle opening of 100% gave the highest efficiency after the remodeling of the turbine (see section 4.4.1 for further details about the remodeling). The distribution of torque indicates that the second stage contributes 7.4 percentage points more to the total amount of transferred torque than the first stage.

The angle, ψ, gives an indication of how many degrees of the runner is utilized per round during the transfer of torque, see figure 5.3. The largest openings have the most extensive angle.

Trends in signal

The calculated data gives information of the percentage distribution of transferred torque during the two stages. But by studying the plots of the filtrated signals, more information about the flow through the runner can be withdrawn.

Figure 6.7 shows a segment of the signal at 100% opening at 250 and 350 *rpm*. Area 1 in the two plots shows a flattening of the signal between the end of the second stage and the start of the first. This is the area where the blades are theoretically empty. When comparing the signal in Area 1 for both speeds one can see that the signal is steeper at 350 *rpm*.

One can observe in figure 6.7 that the value of the valley between peak 1 and peak 2 changes with rotational speed. The turning point of the valley at 250 *rpm* is at almost equal level as the signal in Area 1. However, when increasing the rotational speed the volt value at the turning point of the valley increases. The change in value of the valley with increasing rotational speed is repeated for every nozzle opening.
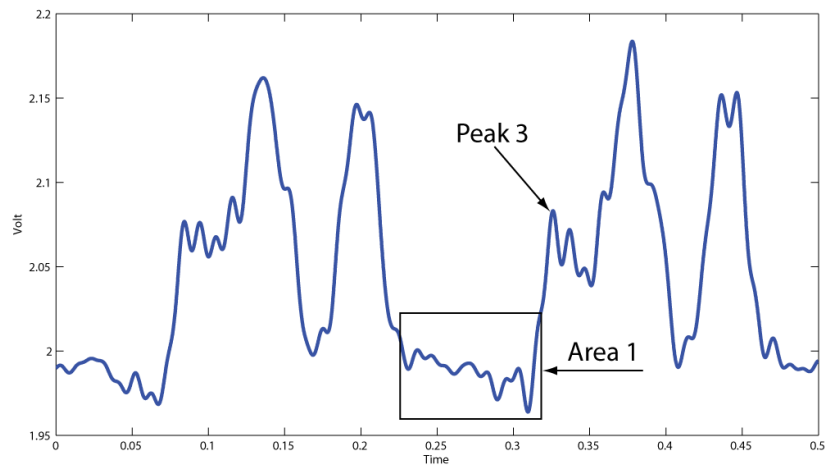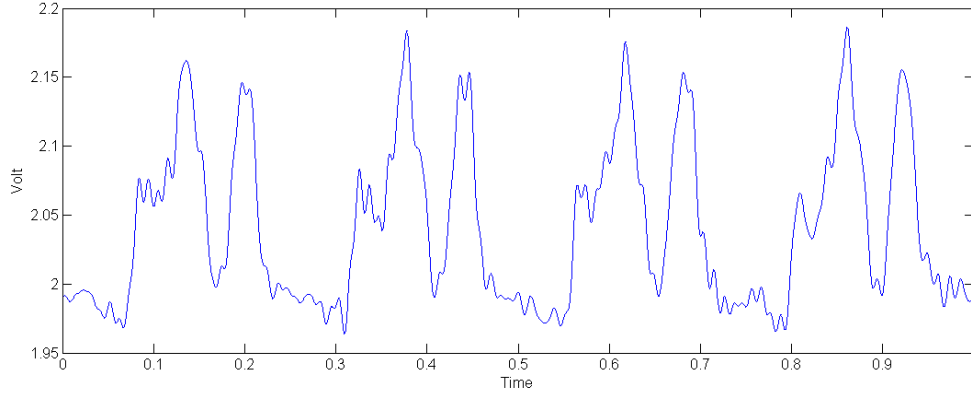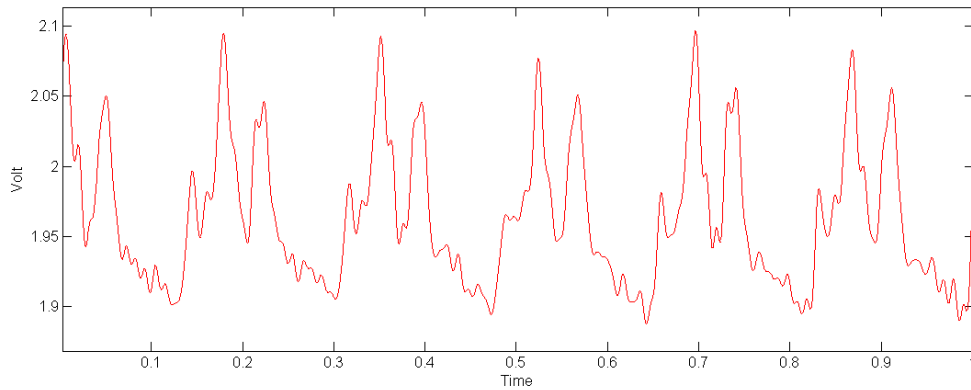
(a) 250 *rpm*
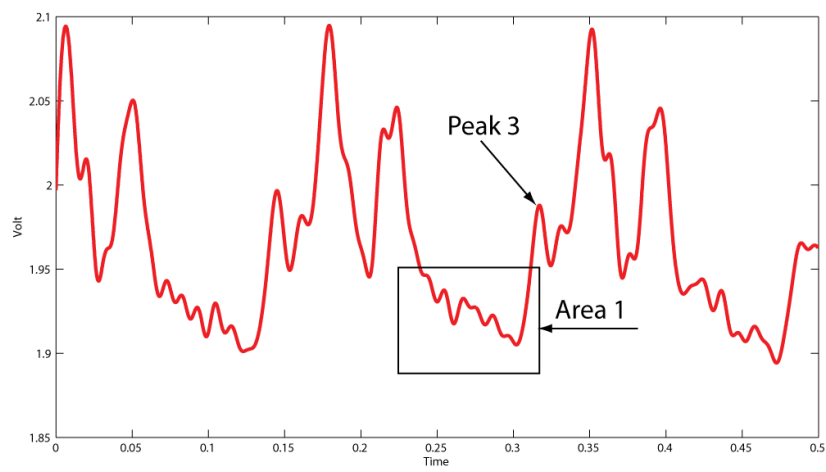
(b) 350 *rpm*

Figure 6.7: Signal for 100% opening

The signal for the 100% nozzle opening stands out from the other openings due to the indication of a third peak, shown as peak 3 in figure 6.7. When calculating the torque transferred during the first stage, peak 3 has been included in the area of peak 1 due to the small valley between them.

(a) 250 *rpm*

(b) 350 *rpm*

Figure 6.8: Filtrated signal for 100% nozzle opening

As the nozzle opening decreases from full opening down to 80%, the peaks become more conspicuous. Figure 6.9 shows that at 350 *rpm* the signal in the period between the end of peak 2 and the start of peak 1 is much more smooth than for 100% opening at the same speed (see figure 6.8).

When comparing figure 6.8 and 6.9, one can see the time interval between the start of the first peak and the end of the second decreases with decreasing nozzle opening. The values for the angle, ψ, shown in table 6.2, supports this observation. The angle decreases with decreasing opening, which means that the water utilize a smaller part of the runner for the torque transfer. The same observation is made for the openings at 60% and 40%.

When decreasing the nozzle opening down to 40%, the signal contains more noise. The peaks are not as clear as for the larger openings, but it is still possible to sort out two peaks of different sizes. Figure 6.10 shows the signal at 40% opening at rotational speed of 250 and 350
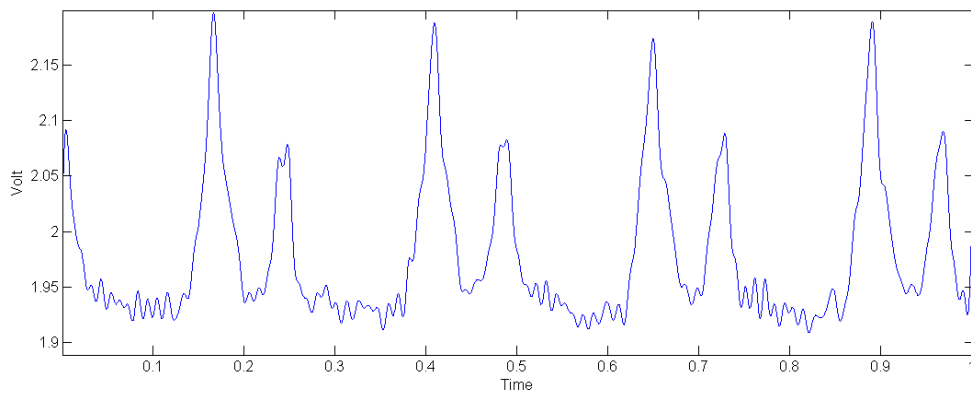
(a) 250 *rpm*
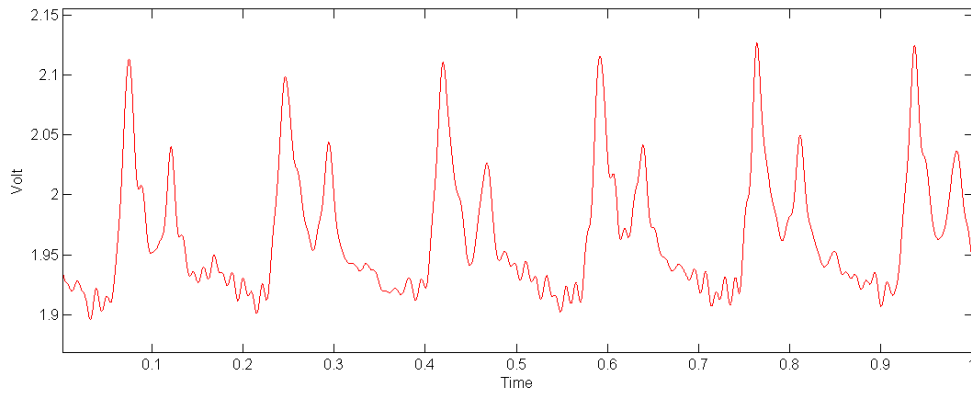
(b) 350 *rpm*

Figure 6.9: Filtrated signal for 80% nozzle opening

rpm. At low rotational speed the second peak is most visible. However, there is an amount of noise between the end of peak 2 and the start of peak 1. When looking at figure 6.10(b), the second peak is about to dissolve. The calculation of contribution from the first and second stage assumed that peak 2 ended in the first valley after the highest point of the peak. Compared to the large openings, there is a significant decrease in efficiency. At 350 *rpm* the efficiency at 40% opening was measured to 58.9%, which is a 16.4 percentage point reduction from the best point of efficiency measured during the strain gage experiment.
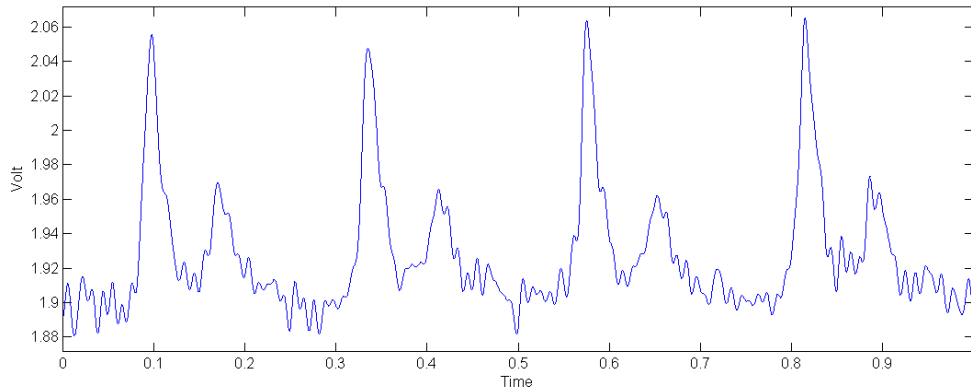
(a) 250 *rpm*
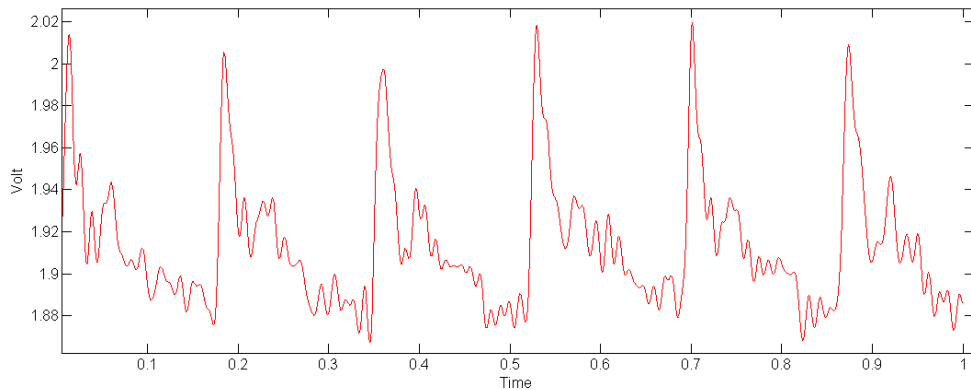
(b) 350 *rpm*

Figure 6.10: Filtrated signal for 40% nozzle opening

The signal for 60% nozzle opening did not show any trends that differ from the ones already explained. A plot of the signal is shown in appendix D.

20% nozzle opening

As mentioned in section 5.2.1, the signal from the tests performed at 20% opening had to be filtrated with a lower frequency than the larger openings. With a filtration frequency of 30 *Hz*, the signal becomes smooth enough to process with the same programs as used for the other openings. However, the start and end points of the peaks are not as accurately

decided, because of the loss of shape in the original signal (see figure 5.4). Table 6.4 shows the distribution of torque transferred during the two stages in the turbine at 20% nozzle opening with a rotational speed of 250 and 350 *rpm*. The distribution shows the same tendency as for nozzle openings larger than 20%. The contribution of the first stage is much larger than for the second, and by increasing the rotational speed the second stage gives a larger contribution than at lower speeds.

	250 *rpm*			350 *rpm*		
Nozzle opening	*First stage*	*Second stage*	ψ	*First stage*	*Second stage*	ψ
20%	66.7%	33.2%	217°	63.2%	36.8%	176°

Table 6.4: Distribution of torque at 20% opening

However, due to the change in filtration frequency when processing the data, this result can only be seen as an indication of distribution.

Chapter 7

Discussion

This chapter goes through the results presented in chapter 6, and tries to determine the specific characteristics of the flow through the runner. The theory behind the losses discussed in this chapter is presented in section 2.3.

7.1   Efficiency

The results from the efficiency measurements performed during the two experiments reveals that the efficiency decreased between the experiments. This change can be explained by the adjustments made on the turbine between the experiments (see section 4.5). The top cover was dismounted in order to remove one of the strain gages and to put more adhesive on the other. The extra layer of adhesive might affect the efficiency. However, the largest loss is most likely caused by the mounting of the Plexiglas plate afterwards. When assembling the Plexiglas plate and the top cover, they were not attached as well as earlier, leading to a small leakage.

The measurements also show a significant variance in results from the flow visualization and strain gage experiments for the efficiency at 60% nozzle opening. The efficiency at this opening increases significantly between the flow visualization and the strain gage experiments. This can be explained by error in the measurements conducted during the flow visualization. When comparing the results with results from the efficiency measurements in 2008 [7] and the measurements during the strain gage experiments, it is highly unlikely that the efficiency at 60% opening contains this amount of variation. Therefore the efficiencies measured at 60% nozzle opening during the flow visualization experiment is rejected.

7.2   Best efficiency point

To obtain the best efficiency point in a cross–flow turbine the turbine should operate with a degree of reaction, which leads to the area between the runner and the top cover to be completely filled. The water enters the blades close to the nozzle outlet, which gives an entrance of the cross flow inside the runner at an early stadium. This characteristic gives good

conditions for the flow through the runner and the direction towards the inlet of the second stage. The incidence loss when the water enters the second stage is low due to the effect of the point of entrance for the cross flow inside the runner. This gives a large contribution of torque transferred through the second stage, which results in only a small amount of remaining energy in the water as it leaves the turbine.

The best efficiency was measured at 100% opening with a rotational speed of 350 *rpm*. This is a change from the efficiency measurements carried out in 2008 [7], where the 80% opening gave the highest efficiency (see section 3.3.2). The change is caused by the remodeling of the turbine (see section 4.4.1). The following discussion is based on the latest measurements. However, it is important to be aware that the highest efficiency of the original turbine design occurs at 80% nozzle opening.

To explain why the efficiency peaks at 100% opening and why it is not higher than 77.5%, one would have to look at the results from the efficiency measurements in 2008 [7], the flow visualization and the strain gage experiment. These three are closely linked. Starting with the experiments from 2008, it was shown that at large nozzle openings the flow rate was reduced with an increase in rotational speed (see section 3.3.2). This gives an indication that the turbine is acting with reaction for openings of 80% and 100%. When operating with reaction there is a positive pressure in the first stage of the turbine, and centripetal forces will slow the water giving a smaller flow rate to the turbine [4]. Due to this positive pressure, a part of the specific energy converted to mechanical energy during the first stage comes from the drop in pressure [5]. The flow pattern through the turbine when operating with a degree of reaction, gives a good indication of why the full opening gives the best efficiency. When looking at figure 6.2(a), it shows that the water enters the blades close to the outlet of the nozzle. This characteristic causes the cross flow to enter the inside of the runner at an early stadium.
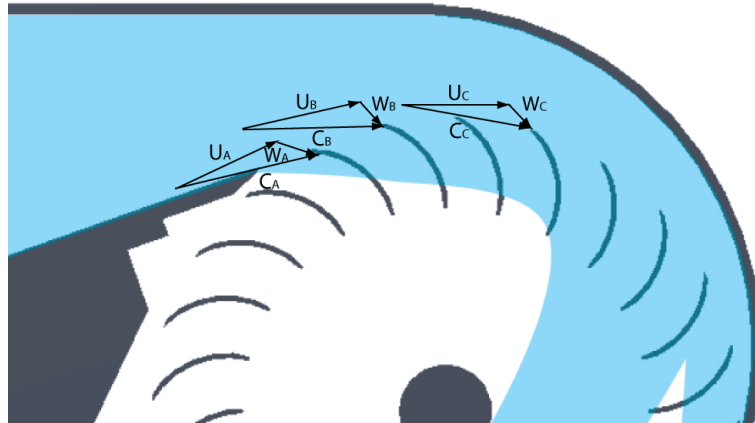
Figure 7.1: Velocity diagrams at the inlet of the runner

At 100% opening the signal from the strain gage measurements indicates a third peak (see figure 6.7). This peak can be explained by studying the velocity diagrams in figure 7.1. The figure shows the change in velocity diagrams at different lengths from the runner. When looking at the diagram with subscript A, the direction of the absolute velocity corresponds well with the rotational speed giving an inflow angle close to the inlet blade angle. The transfer of momentum at this point is the cause of the third peak. The small size of the peak is due

to only a small part of the water entering the runner at this point. However, as the water is distributed further away from the nozzle the velocity diagram (subscript B) shows that less momentum is transferred due to the wrong inflow angle. The change in inflow angle gives a larger amount of incidence losses. This is shown in figure 6.7, by the valley that occurs after peak 3. As the water moves further away from the nozzle, it will again hit the blades with a correct inflow angle (shown in the velocity diagram with subscript C). This result in the large peak occurring after peak 3 (see figure 6.7).

The early entrance of the cross flow inside the runner at best efficiency point causes the water to move almost vertical through the runner before entering the second stage. The distribution of torque (see table 6.2) shows that at full opening and a rotational speed of 350 rpm, the second stage contributes to 53.7% of the total amount of torque transferred through the runner. This indicates that the angle of attack and rotational speed corresponds better at the inlet of the second stage than at the first stage. However, Area 1 in figure 6.7(b) shows that torque is transferred in the area where blades are supposed to be empty. This indicates that the water is entering the second stage with a flow that is spread out due to incidence losses.

At the outlet of the second stage the water changes direction, and leaves with a flow that is close to vertical (see figure 6.3). There is still some remaining energy in the water, which is not utilized, but the amount is significantly lower than for other openings. In addition to this loss, the water that is entrained in the runner is also counted for as a loss. The water contributes to the torque transfer during the first stage, but because the flow does not cross inside the runner towards the second stage, energy is lost.

7.3   Drop in efficiency with decreasing nozzle opening

All experiments performed show that the efficiency drops when the nozzle opening decreases below 80%. The efficiency measurements carried out in 2008 [7] and 2009 show a significant drop between 60–20% nozzle opening. Both the flow pattern and the distribution of the torque transferred, give reasonable explanations for this characteristic.

The efficiency measurements conducted in 2008 [7] show that with openings smaller than 80%, the cross–flow turbine operates as an impulse turbine. It is therefore interesting to note that when the characteristic of the turbine moves over to impulse, the efficiency decreases rapidly. When operating as a pure impulse turbine a larger amount of windage loss occurs (see section 2.3). The magnitude of this loss is not possible to predict at this point, but one should be aware that the loss increases at openings smaller that 80%.

In section 6.1 it is pointed out that the decrease in nozzle opening leads to the cross flow entering the inside of the runner further away from the nozzle outlet. The reason for this is the fact that the water enters the runner at a longer distance from the nozzle exit. The entrance is important due to the angle of attack both on the first and second stage. For example, at 20% opening the flow crosses the inside of the runner almost horizontally, giving a poor angle of attack (see figure 6.2(e)). This causes an increase in incidence losses. The torque distribution shows that at small openings, the first stage contributes more to the total amount of torque transferred, supporting the theory of the angle of attack corresponding poorly to the blade inlet angle at the second stage. In addition, when looking at the plot from

the signal at 40% opening with a rotational speed of 350 *rpm* (see figure 6.2(d)), it shows that the torque is transferred during a longer period and with less momentum during the second stage than for large openings.

For all nozzle openings smaller that 80%, the direction of the absolute velocity at the outlet of the second stage is close to the angle at the inlet. This indicates that only a small amount of energy is extracted during the second stage, which results in a significant amount of energy remaining in the water that does not provide torque to the runner.

In addition to the losses explained above, leakage loss and loss due to entrained flow will affect the efficiency. Due to the experimental setup it is not possible at this time to conclude with the effect of nozzle openings on these losses. However, it can be assumed based on the observations that the amount of leakage and entrained flow does not decrease significantly with decreasing nozzle opening. Therefore, these losses will not be considerably lower than for larger openings.

7.4 Optimum rotational speed

The rotational speed that gives the highest efficiency for all nozzle openings occurs at 350 *rpm*. The reason for this is that the inflow angle at the first and second stage corresponds well with the angle between the blade and the runner periphery at this speed. In addition, there are other types of losses that occur at lower and higher speeds. At a rotational speed of 250 *rpm*, a collision with the shaft is observed for the two largest nozzle openings. The flow pattern through the runner where a collision is observed is shown in figure 6.6(a) and 6.6(b). The decrease in efficiency for openings with collision is significantly larger than for those without a collision (see table 6.1). Therefore the turbine should not be operating at low speed with nozzle openings of 80% and 100%.

When the rotational speed increased to 450 *rpm* during the flow visualization experiment, the efficiency dropped between 6–10 percentage points for each opening. This large drop is explained by the rotational speed not corresponding well with the angle of attack and the inlet angle of the blade, which gives a large amount of incidence losses. In addition, the loss due to entrained flow is observed to increase with increasing rotational speed. Also, the direction of the absolute velocity at high rotational speed is observed close to similar for the water when entering and leaving the second stage. This gives a significant amount of energy left in the water at the turbine outlet.

7.5 Comparison to previous work

When comparing the findings from the two experiments performed in this thesis to the work of other researchers (see section 3.2) the results both agree and disagree.

The flow visualization support Fay and Durgins observation of entrained flow [8]. However, their conclusion that no well defined jet exist inside the runner is contradictory to the observations of the cross–flow turbine used for the experiments in this thesis. At large openings the inside jet is well defined through the runner, and gives a significant distribution of torque

during the second stage. Fay and Durgins experiments using a flow deflector to measure the contribution of the second stage, showed that only 17% of the power was extracted during the second stage. This is a rather different result than what was obtained in the strain gage experiments. At an opening of 40% the second stage showed a contribution of 36.4% at a rotational speed of 250 *rpm*, which is the lowest contribution of all openings tested. This result is based on the 20% opening being excluded from the standard data processing procedure (see section 5.2). It should also be mentioned that the maximum efficiency measured on Fay and Durgins turbine was 61%, while for 40% opening the efficiency was measured to 58.9% during the strain gage experiment. So although the turbine used for the strain gage experiments had a lower efficiency at the point where the contribution from the second stage was at its lowest, the results still showed a higher contribution from the second stage than for Fay and Durgins experiments.

The more recent experiments conducted by Fiuzat and Akerkar [10], in order to identifying the contribution of the two stages of power generation to the shaft power, agreed well with the findings in this thesis. A flow diverter was used to measure the crossing flow, and determining the power output of the two stages (see section 3.2.2). The report concluded that 41% of the power generation occurred during the second stage for a turbine with a nozzle entry arc of 120°. This is the same size arc as on the IAM–turbine. In addition to this conclusion, Fiuzat and Akerkar claim that the contribution of the second stage can be even higher when the flow diverter is not inserted in the turbine. The measurements with a strain gage support this assumption. The highest measured contribution of the second stage was 53.7% at 100% opening with a rotational speed of 350 *rpm*.

When comparing the results from the strain gage experiment to the theoretical predicted distribution of torque (see section 3.3.1), one can see that the results differ substantially from the experimental results. The assumptions made for the theoretical analysis do not include any losses. In addition the analysis assumed, based on the velocity diagram at the inlet of the runner, that the magnitude of the relative and peripheral velocity were equal at the inlet of the first stage. These assumptions do not correspond with the experimental results. Although the relative and peripheral velocity might be close to equal, the losses are far from zero. Therefore, the distribution of the torque during the two stages differs between the theoretical and experimental work.

Chapter 8

Conclusions

In this thesis the flow pattern and torque transfer in a cross–flow turbine is investigated. Two types of experiments have been performed. The first experiment used a single–lens reflex camera and stroboscopes, in order to determine the flow pattern through the runner. The second determined the distribution of torque through the two stages in a cross–flow turbine, with use of strain gages.

The processed data from the two experiments conducted gives valuable information about the cross–flow turbine. The results from the flow visualization experiment resulted in drawings of the flow pattern through the runner. The strain gage measurements gave an overview of the distribution of torque transferred during the two stages in the turbine. When combining the drawings of the flow pattern with the results from the strain gage experiments, the flow characteristics of the cross–flow turbine could be determined.

Based on the results one can conclude that the turbine is efficient at nozzle openings of 80% and 100%. These are the two openings where the turbine works with a degree of reaction. By testing the efficiency at different rotational speeds, 350 rpm proved the most efficient for all nozzle openings. This is the rotational speed which gives the lowest amount of incidence losses at the entrance of the first and second stage. The highest efficiency is obtained for the large nozzle openings where the cross flow enter the inside of the runner at an early stadium. As long as the rotational speed is sufficient, the jet inside the runner does not collide with the shaft. The early entrance of the cross flow results in an angle of attack which corresponds well with the blade inlet angle at the second stage. This results in a minimum amount of incidence losses. The distribution of torque shows that the contribution of the second stage has a large influence on the efficiency. At best efficiency point, the second stage is observed to contribute a greater amount of torque than the first stage.

One can also conclude that the nozzle shape is not optimal for openings of 60% or smaller. The water enters the runner at a significant distance from the nozzle outlet, which gives a late entrance of the cross flow inside the runner. This causes a poor angle of attack at the entrance of the second stage, resulting in an increase in incidence losses.

Chapter 9

Further work

The purpose of this thesis has been to determine the flow pattern through the cross–flow turbine and the distribution of torque during the two stages. However, there is still a large amount of work that can be done on the turbine in order to improve its efficiency. This chapter goes through some suggestions for further work.

The nozzle design of the cross–flow turbine is an area that needs more investigation. The experiments performed in this thesis indicate that the nozzle does not give optimum flow at small nozzle openings. It is therefore of interest to find a nozzle design where the water enters the runner close to the nozzle outlet at all openings without increasing the amount of incidence losses.

The use of interior guide tubes can be a solution to the low efficiency at small nozzle openings. Fiuzat and Akerkar [10] conducted a series of experiments trying to improve the efficiency by the use of guide tubes. The results showed improvement. However, it is important that the guide tubes improve the flow at small nozzle openings without interfering with the flow at larger openings in a negative way.

Experiments with variations in the different design parameters like the number of blades and blade inlet and outlet have not been performed on the IAM–turbine. By retrieving information about these parameters, the turbine design can be improved resulting in a higher efficiency. However, the change in design must not be too advanced, the primitive conditions at the workshops that manufacture the turbine must be accounted for.

Bibliography

[1] Nadim M. Aziz and Venkappayya R. Desai. *An experimental study of the effect of some design parameters on cross-flow turbine efficiency.* Department of Civil Engineering, Clemson University, 1993.

[2] Nadim M. Aziz and Venkappayya R. Desai. *A laboratory study to improve the efficiency of cross-flow turbines.* Department of Civil Engineering, Clemson University, 1993.

[3] O.E. Balje. *Turbomachines: A guide to design, selection and theory.* John Wiley & Sons, Inc, 1981.

[4] Hermod Brekke. *Grunnkurs i hydrauliske strømningsmaskiner.* The Waterpower Laboratory, NTNU, 2000.

[5] Hermod Brekke. *Pumper og Turbiner.* The Waterpower Laboratory, NTNU, 2003.

[6] Paul Clammer. *Afghanistan Travel Guide.* Lonely Planet, 2007.

[7] S.O. Danielsen and E.C. Walseth. Virkningsgradmåling av cross-flow turbin. Project at the Norwegian University of Science and Technology, 2008.

[8] W.W Durgin and W.K Fay. Some fluid flow characteristics of a cross flow type hydraulic turbine. *Small Hydro Power Machinery*, 1984.

[9] A.A. Fiuzat and B. Akerkar. The use of interior guide tube in cross flow turbines. *Waterpower 89*, 2, 1989.

[10] Abbas A. Fiuzat and Bhushan P. Akerkar. Power outputs of two stages of cross-flow turbine. *Journal of Energy Engineering*, 117, 1991.

[11] L.A. Haimerl. The cross-flow turbine. *Water Power Engineering Magazine*, 1960.

[12] Remote HydroLight. http://www.remotehydrolight.com.

[13] International Electrotechical Commission (IEC). *IEC 60193. International standard. Hydraulic turbines, storage pumps and pump-turbines. Model acceptance test.* International Electrotechical Commission, 1999.

[14] C.A. Mockmore and F.Merryfield. The Banki Water Turbine. *Engineering Experiment Station Bulletin No.25, Oregon State College*, 1949.

[15] Torbjørn Kristian Nielsen. *Transient Characteristics of High Head Francis Turbines.* PhD thesis, NTH (The Norwegian University of Science and Technology), 1990.

[16] N.H Costa Pereira and J.E. Borges. Study of the nozzle flow in a cross-flow turbine. *International Journal of Mechanical Sciences*, 38(3), 1996.

[17] Owen Schumacher. Remote Hydrolight turbine test announcement. Handouts, 2009.

[18] D.G. Sheperd. *Principles of Turbomachinery*. Macmillan Publishing CO., INC, 1956.

[19] S.Khosrowpanah, M.L. Albertson, and A.A Fiuzat. Experimental study of cross-flow turbine. *Journal of Hydraulic Engineering*, 112(3), 1988.

[20] Pål-Tore Selbu Storli. Modelltest av Francis Turbin i Vannkraftlaboratoriet ved NTNU. Master's thesis, NTNU, 2006.

[21] P.A Tipler. *Physics for scientists and engineers*. W.H Freeman and Company, 4th edition, 1999.

[22] A.J. Wheeler and A.R.Ganji. *Introduction to Engineering Experimentation*. Pearson Education, Inc., 2nd edition, 2004.

[23] Young and Freedman. *University Physichs with Modern Physics*. Pearson Education Inc., 11th edition, 2004.

Appendix A

Travel report

Purpose of the trip

In the fall of 2008 a cross–flow turbine manufactured by Remote HydroLight in Afghanistan was installed in the Waterpower Laboratory at the Norwegian University of Science and Technology. During the fall efficiency measurements were carried out, giving a maximum efficiency of 78.6%. Although the efficiency is high for a turbine with such a simple design, there is a desire to improve it in order to utilize the resources better. This thesis has been focusing on the flow pattern through the turbine, and the distribution of torque transferred during the two stages. As a preparation for the experiments, a trip to Afghanistan was conducted in February 2009. The purpose of the trip was to learn more about the cross–flow turbine and the manufacturing methods used by Remote HydroLight.

About Afghanistan

Located in the centre of Asia Afghanistan is surrounded by Pakistan, China, Tajikistan, Uzbekistan, Turkmenistan and Iran. The country had in 2006 an estimated population of 31 million, with approximately 14 million under the age of 14. Before the 21st century Afghanistan was widely known for its dramatic mountain scenery and the unparalleled hospitality of its people. Today the country is synonymous with war and terrorism.

Since the late 1970s Afghanistan has more or less been suffering by continuous civil war and foreign invasions. The Soviet Union invaded Afghanistan in 1979, initially they expected to be there just a few months but events soon spiraled out of their control. This was the start of a ten year long war. In 1989 the Soviets pulled back their troops giving their support to the new government, hoping it would survive This did not happen, in 1992 Kabul was captured by a resistance known as the the mujaheddin, triggering the start of civil war. The Taliban militia formed in 1994 and quickly gained control over several cities in Afghanistan. In 1996 Kabul were captured and the Islamic Emirate of Afghanistan were established. The Taliban implemented the strictest interpretation of Sharia law ever seen in the Muslim world. Women were banned from jobs, girls forbidden to attend schools and universities and thieves were punished by amputating one of their hands or feet. The Taliban remained in control until 2001, when U.S-led troops invaded Afghanistan and forced Taliban out. The invasion came as

a response to the 9/11 attack on the World Trade Center in New York, and the Americans hunt for Osama Bin Laden. In 2002 the Americans with support from other nations started the reconstruction of Afghanistan. At this point people were traumatized and all infrastructures were destroyed. Security was top priority in addition to establish a viable afghan government. In 2004 a new constitution were signed and Hamid Karzai were elected president, and is still reigning.[6]

Today Afghanistan is still far from rebuilt, but there are examples of signs of progress; the citizens of Kabul have just recently experienced the joy of having available electricity 24 hours a day. Electricity is an important part of developing the country, and the focus is now on getting electricity out to the small villages.

About Remote HydroLight

Remote HydroLight is an Afghan company involved in training, manufacturing and installing of micro-hydropower plants throughout Afghanistan. The company has 11 employees, 9 Afghans, one American and one Norwegian. Their hydropower services help private workshops and villages to build community owned and maintained electric power plants [12]. In the heart of Kabul the Remote HydroLight workshop lies between carpet sellers and bakeries. The workshop is of high standard compared to other workshops in Kabul. Most of the work takes place indoors, every day the workers get a warm lunch prepared by a chef and the salary is good compared to other occupations.

Figure A.1: Lunch at the workshop

Villages come to Remote HydroLight wanting help to finance, build and learn how to maintain a hydropower plant. The company checks the area to see if and what type of cross-flow turbine it is suited for, before a deal between the company and the village is put together.

It is of great importance that the village takes part in the building of the plant, and they are often responsible for the building of the channel. Remote HydroLight prepare a budget which includes all the costs of production and building of a hydropower plant. This budget is handed over to the U.S Core of Engineers who will finance the project if approved.

Production of cross-flow turbine

The turbine design was developed under the International Assistance Mission (IAM) in 1998. Remote HydroLight have developed the design further to include labor saving features to help local workshops produce a high quality turbine at a reasonable price without compromising efficiency. To date approximately 1300 of the IAM turbines have been built by private Afghan workshops [17].

Remote HydroLight manufactures three variations of the cross-flow turbine:

Name	*Abbreviation*	*Rotor diameter*	*Electrical output*
Traditional Mill Turbine	TMT	$0.27\,\mathrm{m}$	$1 - 14\,\mathrm{kW}$
Hindu Kush Turbine	HKT	$0.34\,\mathrm{m}$	$8 - 55\,\mathrm{kW}$
Pamir Turbine	PM	$0.34\,\mathrm{m}$	$36 - 120\,\mathrm{kW}$

Table A.1: Table of different turbine types

The TMT–turbine is the one used for the experiments performed in this thesis. It consists of a lower frame, turbine casing, runner and an adjustable nozzle. The following will give a brief review of how the manufacturing process of this turbine works.

The lower frame exist of four 14 *cm* C-channels welded together. Holes are drilled around the frame in order to attach the turbine casing. The runner consists of a shaft, four circular plates and blades. The shaft is cut on the lathe into proper dimensions. Then the four circular plates are welded on. The end plates have scratched on marks for where the 24 blades are to be welded. The blades trailing edge is grinded by hand before welded on to the runner, and the leading edge is grinded after attachment. The assembled runner is then cut in the lathe to obtain the correct diameter. When the runner is complete, it is mounted on to the lower frame together with the bearings and bearing holders. The circular arc on the top cover of the turbine is then made and tacked on to the lower frame. The straight piece from the arc to the turbine inlet is then welded on. A rectangular inspection hatch is cut out from the straight piece. When the turbine casing is complete, the adjustable nozzle is installed. With all parts in place a final welding is performed on the casing to ensure a high strength and no leakages.

In addition to the cross-flow turbine, trash racks, gates and control systems are also produced at the shop. The material and needed parts is imported from other countries. Remote HydroLight mainly import from Pakistan, Russia and China. The blades in the runner are made in Pakistan; this is to ensure that they are as perfectly shaped as possible in order to maintain a good efficiency. Steel for the turbine casing is imported from Pakistan and Russia. Bearings for the runner are either Russian or Chinese, while the bearing holders are imported from Pakistan.

The cross-flow turbine uses a belt drive to transfer shaft power to the alternator. The pulleys and belts used for the transfer are imported from Pakistan. Depending on the electrical output number of belt drives and belts are decided.

In addition to manufacturing turbines the workshop produces and imports other parts of a hydropower plant as well. The control system is put together in the workshop with imported parts from Pakistan and the Philippines. The generator is made in China. Pulleys to connect the turbine to the generator are imported from Pakistan. Trash racks and gates are produced at the workshop with material from mainly Pakistan and Russia. Pipes to the hydropower station are imported from Pakistan if they are smaller than 12 *inches*, if bigger the workshop makes them out of metal plates.

Other workshops in Kabul

There are several workshops producing the cross-flow turbine in Kabul. Most of them are trained by Remote HydroLight and are using the IAM turbine design in their production. The workshops sell their turbines to the National Solidarity Programme (NSP), who sponsor hydropower plants in small villages, or to private households.

A basic workshop in Kabul has just enough equipment and roof over its head to produce cross–flow turbines, trash racks, gates and control systems. The workers stand outside in the cold from early morning to late night working on the turbine. Each workshop has 8-10 mechanics employed and are capable of producing equipment for one power plant a week.

The hydropower plant in Panjshir Valley

Panjshir Valley is known as one of the most beautiful spots in Afghanistan, and in the 1970s it was a popular tourist destination. Located north of Kabul the valley spans out over 100 *km*.

In co-operation with Remote HydroLight a couple of the villages in the valley have built four new hydropower plants. The biggest plant is located at Daste Riwat in Panjshir, and this is the largest project Remote HydroLight has done. The building started in 2008, and is now running continuously. The Daste Riwat plant has two Pamir turbines installed. The turbines are expected to deliver 70kW each with full flow, giving enough power for 200 families. In Afghanistan each family have approximately six members, which means that 1200 people get their electricity from this plant.

Figure A.4 gives an overview of the plant and some of its consisting elements. The channel with a length of 1.8 *km* was built by the village. The gate in figure A.4(c) is used to water the fields when necessary, and in the same picture the overflow system is shown. This system was especially manufactured by Remote Hydrolights workshop for the Daste Riwat plant. The net head is approximately 15.5 *meter* and full flow is estimated to 750 L/s. Inside the power station two Pamir turbines are installed. Heavy duty bearings are used on this turbine to allow belt drives from both sides of the turbine, which simplifies the transfer of shaft power to the alternator.

(a) Worker by a lathe

(b) Welding

(c) Control system

(d) Drilling

(e) Pipe cutting

Figure A.2: Workers at Remote HydroLight workshop

Further up the river from Daste Riwat there are three hydropower plants equipped with TMT turbines.

Furthest up is a plant with a TMT turbine. It operates with e net head of 9 *meter* and a flow rate of 180 *L/s*. The plant delivers approximately 10 *kW* which provides electricity for about 40 houses or 240 people. Downstream from this plant, two smaller plants with 4 *meter* head lies in a row. Both plants produce approximately 3 *kW* each, which supplies about 25 households. Both plants have a flow rate at 160 L/s at full flow. The cost of a plant at this size is about 10000 US, which include all cost to build the plant. Electrical equipment inside houses is not included in this cost. The power is mostly used for light in the houses, some also have a television and kitchen equipment.

Figure A.3: Old waterwheel in the Panjshir Valley

(a) The Hydropower Plant

(b) Channel

(c) Overflow with gate for applying water to fields

(d) Pamir Turbine

(e) Control system

Figure A.4: Daste Riwat Hydropower Plant

Appendix B

Uncertainty analysis

The uncertainty analysis is based on the method described in Storli [20] and the calculations performed by Danielsen and Walseth in 2008 [7].

Equations

The relative uncertainty, f_x, of a measurement can be expressed as:

$$f_x = \frac{e_x}{X} \tag{B.1}$$

e_x – Absolute uncertainty in measurement of X

X – The measured quantity

To find the uncertainty in the efficiency measurements, one would have to use the root-sum-square method. With use of equation 2.2, the expression for the uncertainty in the efficiency measurements is derived:

$$f_\eta = \sqrt{f_\rho^2 + f_g^2 + f_{H_e}^2 + f_Q^2 + f_T^2 + f_\omega^2} \tag{B.2}$$

f_ρ – Uncertainty in the density of the water

f_g – Uncertainty deciding the gravitational constant

f_{H_e} – Uncertainty in calculated net head, see equation B.3

f_Q – Uncertainty in measured volume flow rate

f_T – Uncertainty in measured torque

f_ω – Uncertainty in measured rotational speed

The expression of the uncertainty of the measured net head is derived from equation 2.3:

$$f_{H_e} = \pm \frac{\sqrt{\left(\frac{e_{\Delta p}}{\rho g}\right)^2 + (e_z)^2 + \left(\frac{e_{v_1}^2}{2g}\right)^2}}{H_e} \tag{B.3}$$

$e_{\Delta p}$ – The absolute systematic error for the pressure, see equation B.4

e_z – The absolute systematic error for the measured difference in height, Z.

e_{v_1} – The absolute systematic error for the velocity at the turbine inlet,see equation B.5

$$\frac{e_{\Delta p}}{\rho g} = \frac{\Delta p}{\rho g} f_{p,tot} \tag{B.4}$$

$$\frac{e_{v_1}}{g} = \frac{v_1^2}{g} f_{v_1} \tag{B.5}$$

Uncertainty analysis separates systematic and random error, the relationship between these can be expressed as:

$$f_\eta = \sqrt{f_{systematic}^2 + f_{random}^2} \tag{B.6}$$

$f_{systematic}$ – Systematic uncertainty in measuring devices, see table 4.1

f_{random} – Random uncertainty in measurements, calculated with equation B.7

The random uncertainty is calculated with the logged signals for each operating point.

$$f_{random} = \frac{S_y t}{\bar{Y}_\eta \sqrt{n}} \tag{B.7}$$

S_y – Standard deviation, see equation B.8.

$\bar{Y}_\eta$ – Aritmetic mean value

n – Number of measurements

t – Student t distribution

$$S_y = \sqrt{\frac{\sum_{i=1}^n \left(Y_i - \bar{Y}\right)^2}{n-1}} \tag{B.8}$$

Y_i – Individual measurement

Calculations

When calculating the uncertainty of the efficiency measurements, the following assumptions were taken:

$f_\rho = 0$ – Small compared to the other uncertainties

$f_g = 0$ – Small compared to the other uncertainties

The values for the systematic uncertainty in the measuring devices, f_Q, f_T and f_ω, were calculated by Danielsen and Walseth [7], and is given in table 4.1. In addition the uncertainty, e_z, was calculated to $\pm 0.5 \ mm$.

The calculated uncertainty of the efficiency measured during the flow visualization and strain gage experiments at a rotational speed are shown in the following tables.

Uncertainty in efficiency measurements during flow visualization

Nozzle opening	Efficiency	Uncertainty
100%	70.6%	±2.87%
80%	67.3%	±3.29%
60%	44.8%	±1.43%
40%	55.1%	±2.84%
20%	45.1%	±3.43%

Table B.1: Uncertainty in efficiency at 450 *rpm*

Nozzle opening	Efficiency	Uncertainty
100%	77.5%	±1.96%
80%	76.8%	±0.87%
60%	60.2%	±0.95%
40%	64.7%	±2.83%
20%	54.9%	±2.85%

Table B.2: Uncertainty in efficiency at 350 *rpm*

Nozzle opening	Efficiency	Uncertainty
100%	69.3%	±1.05%
80%	70.5%	±1.86%
60%	61.7%	±1.68%
40%	61.6%	±1.37%
20%	53.7%	±1.37%

Table B.3: Uncertainty in efficiency at 250 *rpm*

Uncertainty in efficiency measurements during strain gage experiment

Nozzle opening	Efficiency	Uncertainty
100%	67.6%	±0.86%
80%	67.4%	±2.56%
60%	63.7%	±2.77%
40%	56.2%	±3.87%
20%	43.8%	±3.57%

Table B.4: Uncertainty in efficiency at 250 *rpm*

Nozzle opening	Efficiency	Uncertainty
100%	75.3%	±0.86%
80%	73.4%	±1.10%
60%	66.9%	±1.83%
40%	58.9%	±2.47%
20%	46.0%	±1.06%

Table B.5: Uncertainty in efficiency at 350 *rpm*

Comment

The uncertainty varies significantly with nozzle opening and rotational speed. In order to find the source of these variations one must perform a time consuming investigation of the results and the instrumentation. However, because the efficiency is not the main objective in this thesis, this type of investigation is not carried out.

Appendix C

Torque transfer

The derivation of the equation for distribution of torque transfer during the two stages in a cross–flow turbine starts with Newton's second law:

$$dF_X = dm\frac{dC_X}{dt} \tag{C.1}$$

Change in mass can be expressed as:

$$dm = \rho Q dt \tag{C.2}$$

Combining equation C.1 and C.2, the following expression emerge:

$$dF_X = \rho Q dC_X \tag{C.3}$$

The reaction force can be expressed as:

$$R_X = -F_X \tag{C.4}$$

Combining equation C.3 with C.4 gives:

$$R_X = \int_2^1 \rho Q dC_X = \rho Q \left(C_{1X} - C_{2X} \right) \tag{C.5}$$

Expressed as vectors:

$$\vec{R} = \rho Q \left(\vec{C_1} - \vec{C_2} \right) \tag{C.6}$$

Definition of torque:

$$T = R \cdot a \tag{C.7}$$

Combining equation C.6 and C.7.

$$\vec{T} = \rho Q \left(\vec{C_1} \times \vec{a_1} - C_2 \times \vec{a_2} \right) \tag{C.8}$$

a_1 and a_2 can with use of geometry be expressed:

$$\vec{a_1} = R_1 \cos \alpha_1 \tag{C.9}$$

$$\vec{a_2} = R_2 \cos \alpha_2 \tag{C.10}$$

Combining equation C.8 with the expression for a_1 and a_2.

$$\vec{C_1} = \frac{C_{u1}}{\cos \alpha_1} \tag{C.11}$$

$$\vec{C_2} = \frac{C_{u2}}{\cos \alpha_2} \tag{C.12}$$

Torque transferred during the first stage:

$$T_{1 \to 2} = \rho Q \left(C_{u1} R_1 - C_{u2} R_2 \right) \tag{C.13}$$

Torque trasferred during the second stage:

$$T_{3 \to 4} = \rho Q \left(C_{u2} R_2 \right) \tag{C.14}$$

Assuming:

$$W_1 = U_1 \tag{C.15}$$

This gives:

$$C_{u1} = U_1 + W_1 cos \beta_1 \tag{C.16}$$

$$U_2 = C_{u2} = C_{u3} \tag{C.17}$$

$$U = \omega R_1 \tag{C.18}$$

The expression for the distribution of torque transferred during the first and second stage:

$$\frac{T_{1 \to 2}}{T_{3 \to 4}} = \frac{R_1^2 (1 + \cos \beta_1) - R_2^2}{R_2 R_1} \tag{C.19}$$

Known values:

- $\beta_1 = 30°$
- $\beta_2 = 90°$
- $R_1 = 0.135 \; meter$
- $R_2 = 0.094 \; meter$

By inserting the known values into equation C.19

$$\frac{T_{1 \to 2}}{T_{3 \to 4}} = 2.85 \tag{C.20}$$

Appendix D

Strain gage signal at 60% nozzle opening
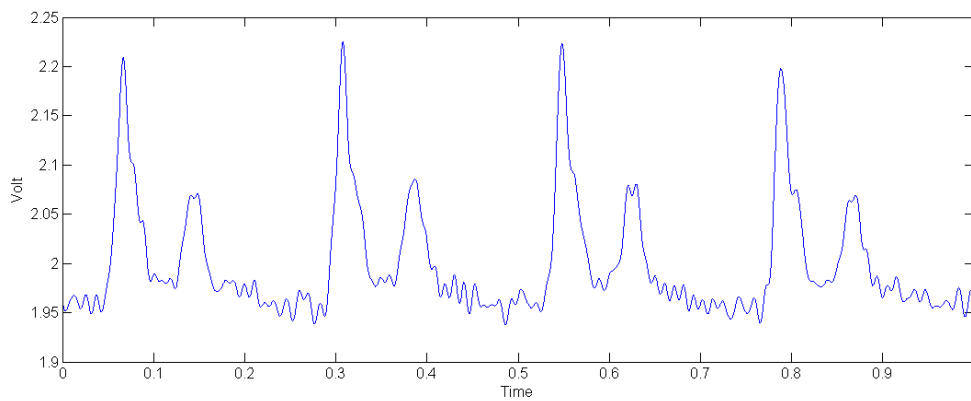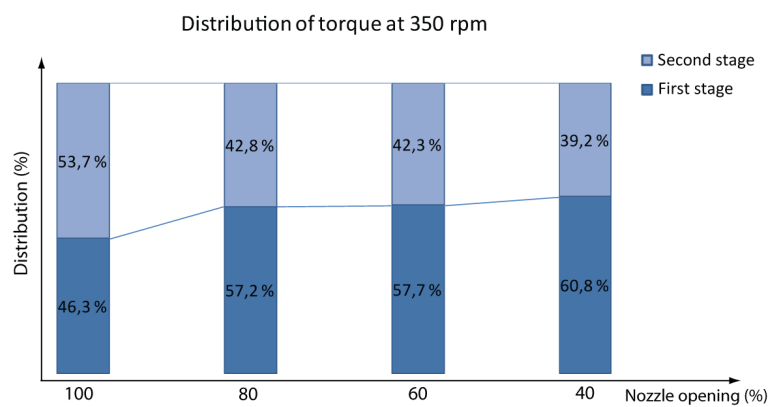

(a) 250 *rpm*
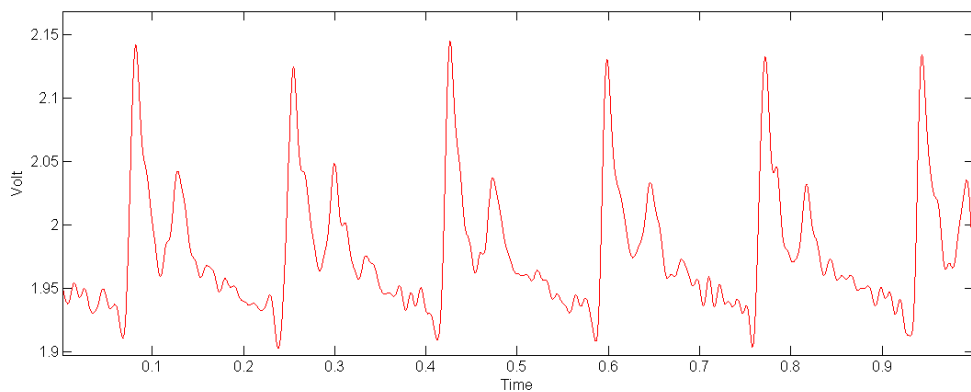
(b) 350 *rpm*

Figure D.1: Filtrated signal for 60% nozzle opening

Appendix E

Distribution of torque
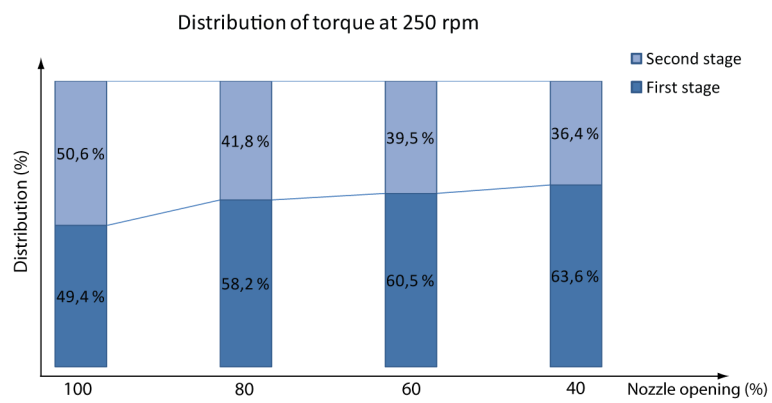
(a) 250 rpm

(b) 350 rpm

Figure E.1: Distribtuion of torque transferred

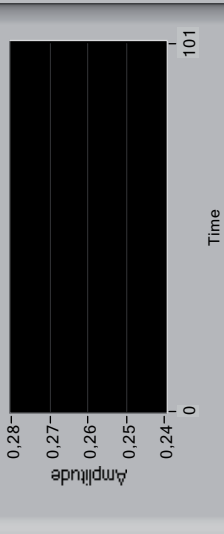# Appendix F

Labview program for measuring efficiency

Tab Control

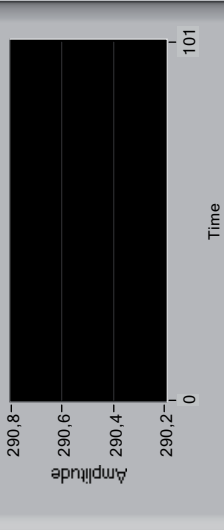Efficiency

output variable

Net Head

e
p_pa
omega
v1
D
D1
rho
ned
Qed
g
deltaz
Heff
Pm
Ph

p_pa=10**5*p;
omega=2*pi*n/60;
v1=(4*Q)/(pi*0.25*0.25);
rho=1000;
g=9.82146516;
D1=0.25;
D=0.27;
deltaz=0.11;
Heff=(p_pa/(rho*g))+deltaz+((v1**2)/(2*g));
Pm=T*omega;
Ph=rho*g*Q*Heff;
e=Pm/Ph;
ned=(n*D)/sqrt(g*Heff);
Qed=Q/(D**2*sqrt(g*Heff));

GJENNOMSNITTSVERDI TIL DISPLAY

Pressure
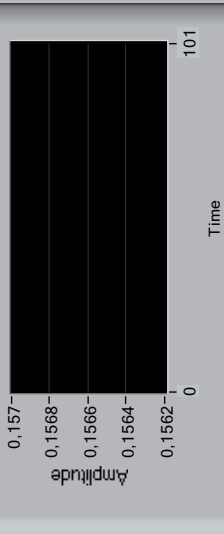
Temperature of water

Torque

Rotational speed

Volume flow rate

KALIBRERING

Moment

subarray

Scans

ScanRate

True

Save

Path

Trykk(bar)
Temp
Moment
RPM
Q
Virkn
ned
Qed
P_turb
P_hydr
P_pa
V1
Heff

p
T
n
Q
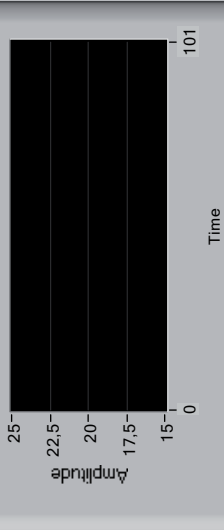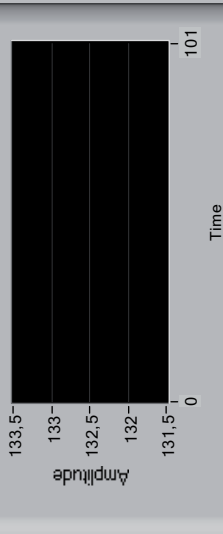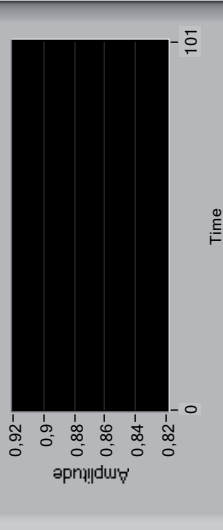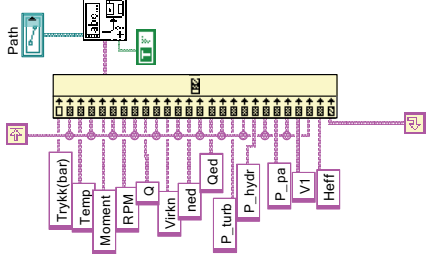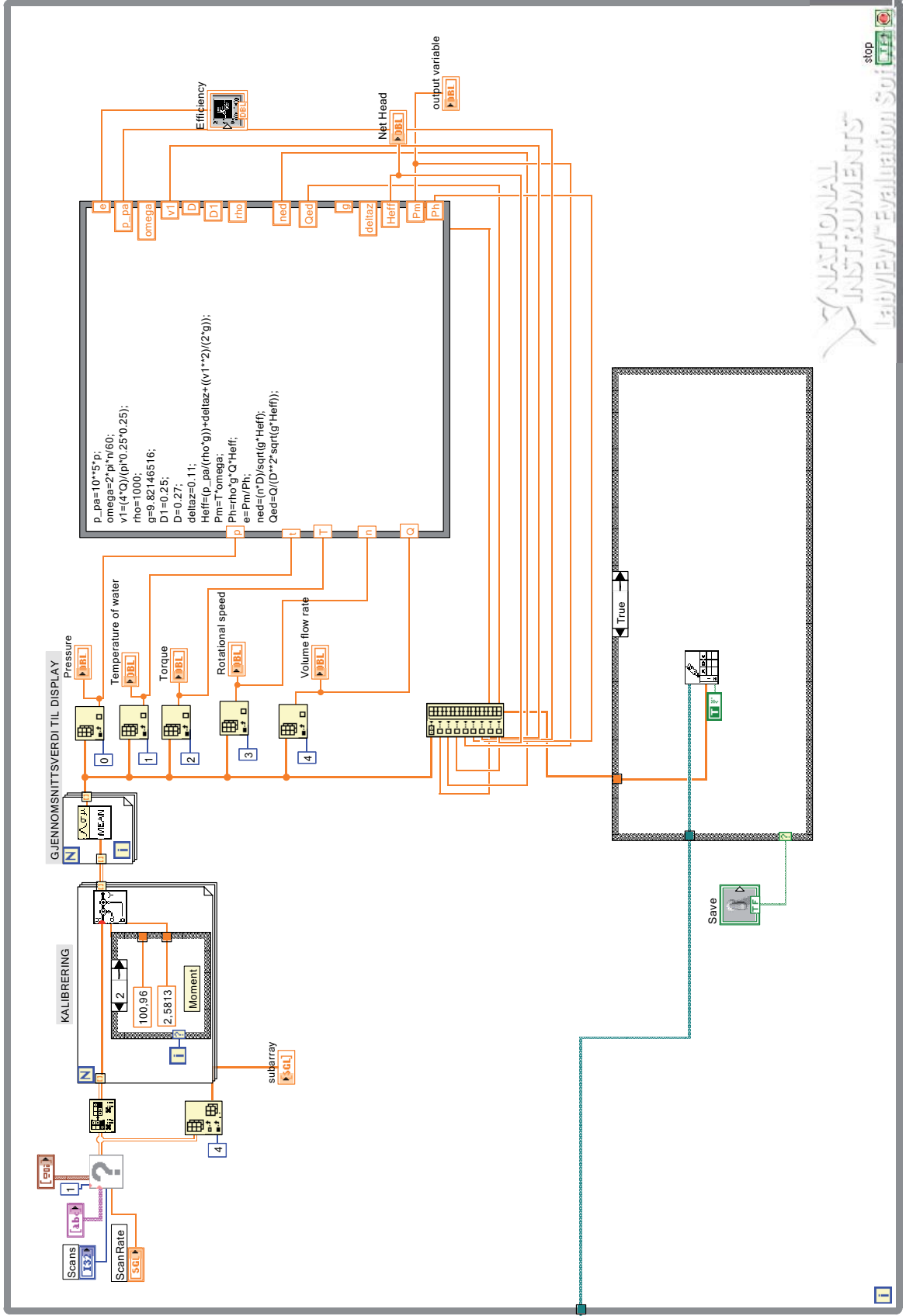
Appendix G

Labview program for logging strain gage signal

Appendix H

Labview program for integrating area under curves

Waveform Graph

Plot 0

Amplitude

2,14
2,12
2,1
2,08
2,06
2,04
2,02
2
1,98
1,96
1,94
1,92
1,9
1,88

0 250 500 750 1000 1250 1500 1750 2000 2250 2500 2750 3000 3250 3500 3750 4000

Time

X-vals New
1,948175E+0
1,946464E+0
1,944785E+0
1,943149E+0
1,941568E+0
1,940051E+0
1,938608E+0
1,937245E+0
1,935971E+0
1,934788E+0
1,933701E+0
1,932711E+0
1,931818E+0
1,931021E+0
1,930317E+0
1,929700E+0
1,929165E+0
1,928704E+0
1,928311E+0
1,927976E+0
1,927689E+0
1,927442E+0
1,927224E+0
1,927025E+0

Lo Pass Filter Frequency
100

Sampling Frequency
4000

Shift 2nd Peak
199

Ekspander
1

Ekspansjon fordeler seg likt
rund toppen på primærpunkt

Lengde 1ste integral
184

Lengde 2ndre integral
146

Peak threshold
2,09

NBI Må tilpasses signalet (se over)

Peaks- Loc & Ampl
298,427222E+0 2,113036E+0
986,062695E+0 2,098194E+0
1,677547E+3 2,110322E+0
2,367501E+3 2,115556E+0
3,056881E+3 2,126995E+0
3,749359E+3 2,124632E+0
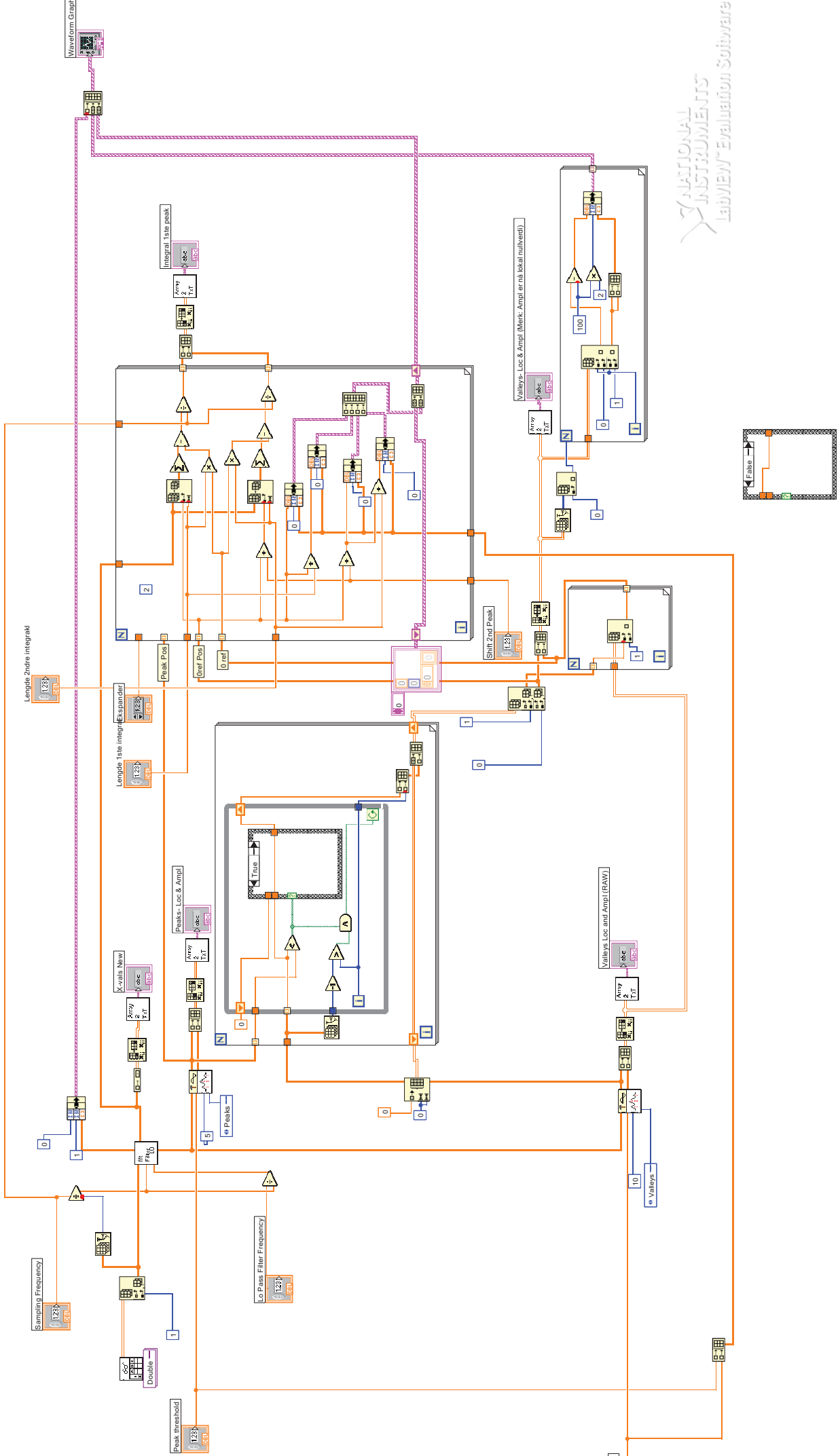
Valley threshold
1,93

NBI Må tilpasses signalet (se over)

Valleys- Loc & Ampl (Merk: Ampl er nå lokal nullverdi)
216,958991E+0 1,926936E+0
903,378544E+0 1,920170E+0
1,601089E+3 1,928973E+0
2,281507E+3 1,929232E+0

Valleys Loc and Ampl (RAW)
47,983928E+0 1,919812E+0
128,743685E+0 1,895952E+0
178,685509E+0 1,902831E+0
216,958991E+0 1,910217E+0
602,318037E+0 1,926936E+0
646,566521E+0 1,929644E+0
730,528896E+0 1,924239E+0
776,351674E+0 1,911713E+0
822,219164E+0 1,916004E+0
859,550328E+0 1,901242E+0
903,378544E+0 1,912418E+0
1,417034E+3 1,920170E+0
1,444109E+3 1,918409E+0

Integral 1ste peak
3,631395E-3 1,896507E-3
4,317921E-3 2,413916E-3
4,030111E-3 1,790905E-3
3,924033E-3 2,328407E-3
4,454042E-3 2,660196E-3
4,552960E-3 2,810462E-3

Appendix I

Matlab program

```
clear all
clc

X=xlsread('a80r350f100', 'a80r350f100', 'A1:A4000');
Y=xlsread('a80r350f100', 'a80r350f100', 'D1:D4000');
plot(X,Y)
%Plots the filtrated signal


    i_min1=[0 0 0 0];
    i_max1=[0 0 0 0];
    i_min2=[0 0 0 0];
    i_max2=[0 0 0 0];
    x_mint1=[0 0 0 0];
    x_maxt1=[0 0 0 0];
    x_mint2=[0 0 0 0];
    x_maxt2=[0 0 0 0];


for k=1:1:4
 keyboard %The program pauses, giving the user time to locate the start
          %and end of the peaks by use of the Data Cursor Tool

    x_mint1(k)=x_min1.Position(1,1)
    x_maxt1(k)=x_max1.Position(1,1)

    x_mint2(k)=x_min2.Position(1,1)
    x_maxt2(k)=x_max2.Position(1,1)


    g=1
    c=1
    b=1
    a=1


%Calculates the average value of the time intervall for peak 1
    while (X(g)≤x_mint1(k))
```

```
        g=g+1
        if X(g)==x_mint1(k)
            i_min1(k)=g
        end
    end

    while (X(c)≤x_maxt1(k));
        c=c+1;
        if X(c)==x_maxt1(k);
            i_max1(k)=c;
        end
    end

%Calculates the average value of the time intervall for peak 2
    while (X(b)≤x_mint2(k))
        b=b+1
        if X(b)==x_mint2(k)
            i_min2(k)=b
        end
    end

    while (X(a)≤x_maxt2(k));
        a=a+1;
        if X(a)==x_maxt2(k);
            i_max2(k)=a;
        end
    end




end

G11=X(i_min1(1,1):i_max1(1,1));
G12=X(i_min1(1,2):i_max1(1,2));
G13=X(i_min1(1,3):i_max1(1,3));
G14=X(i_min1(1,4):i_max1(1,4));
grenseverdi_tid1=mean([G11; G12; G13; G14])

G21=X(i_min2(1,1):i_max2(1,1));
G22=X(i_min2(1,2):i_max2(1,2));
G23=X(i_min2(1,3):i_max2(1,3));
G24=X(i_min2(1,4):i_max2(1,4));
grenseverdi_tid2=mean([G21; G22; G23; G24])

%Calculates the mean value for the time interval
grenseverdi_indeks1=mean([i_max1(1,1)−i_min1(1,1);i_max1(1,2)−i_min1(1,2);
    i_max1(1,3)−i_min1(1,3);i_max1(1,4)−i_min1(1,4)])
grenseverdi_indeks2=mean([i_max2(1,1)−i_min2(1,1);i_max2(1,2)−i_min2(1,2);
    i_max2(1,3)−i_min2(1,3);i_max2(1,4)−i_min2(1,4)])

%Calculates the mean value for the time intervall between the start of peak
%one and the start of peak 2
 shift2ndpeak=(i_max1−i_min1)+(i_min2−i_max1)
 secondpeak=mean(shift2ndpeak)
```

```
% Combining the values in a matrix
samleverdier=[i_min1;i_max1;i_min2;i_max2;x_mint1;x_maxt1;x_mint2;
    x_maxt2;shift2ndpeak]
% Making a vector of the average values
snittverdier=[grenseverdi_tid1;grenseverdi_tid2;grenseverdi_indeks1;
    grenseverdi_indeks2;secondpeak]
% Combining the time series and the filtrated signal in a matrix
inndata=[X Y]


%Writing the calculated values, mean values and the signal to an excel
%file for further processing
xlswrite('80350', inndata, 'inndata')
xlswrite('80350', samleverdier, 'samleverdier')
xlswrite('80350', snittverdier, 'snittverdier')
```

Appendix J

IAM–turbine design
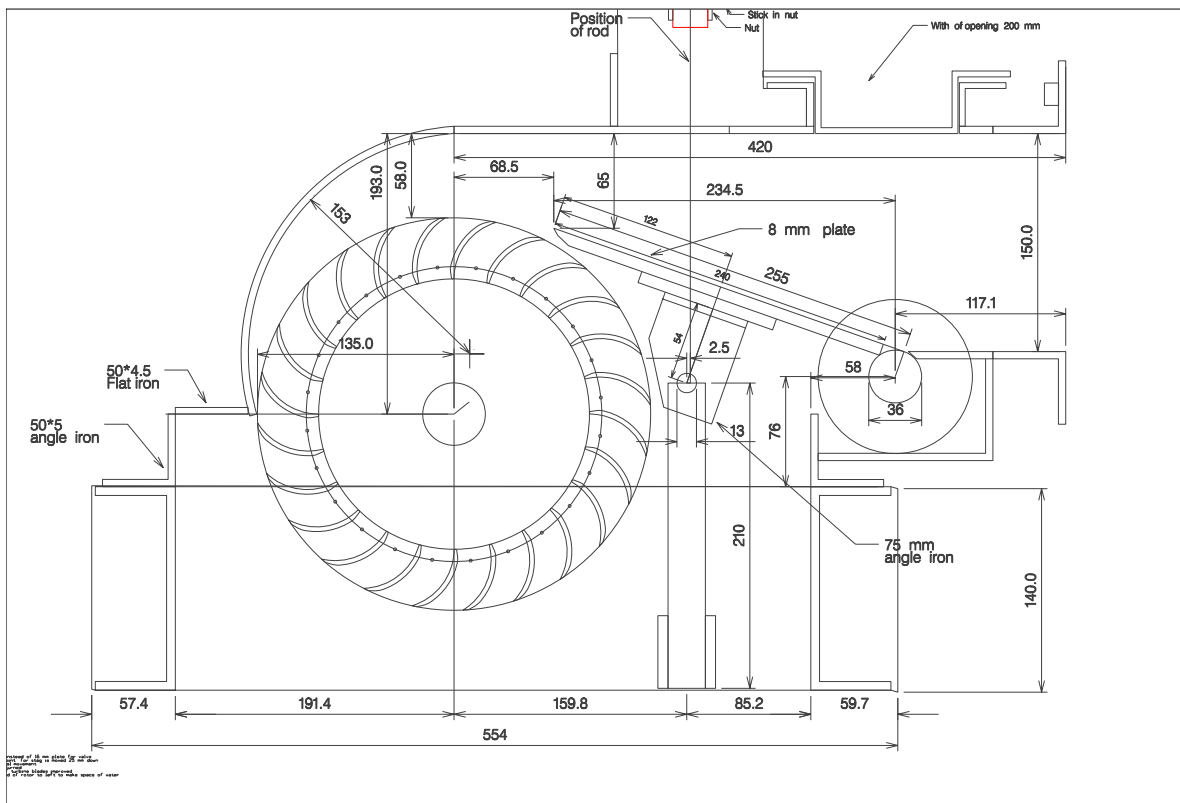
Appendix K

Pictures from the flow visualization experiment

Figure K.1: 20% nozzle opening at a rotational speed of 350 *rpm*

Figure K.2: 20% nozzle opening at a rotational speed of 350 *rpm*

Appendix L
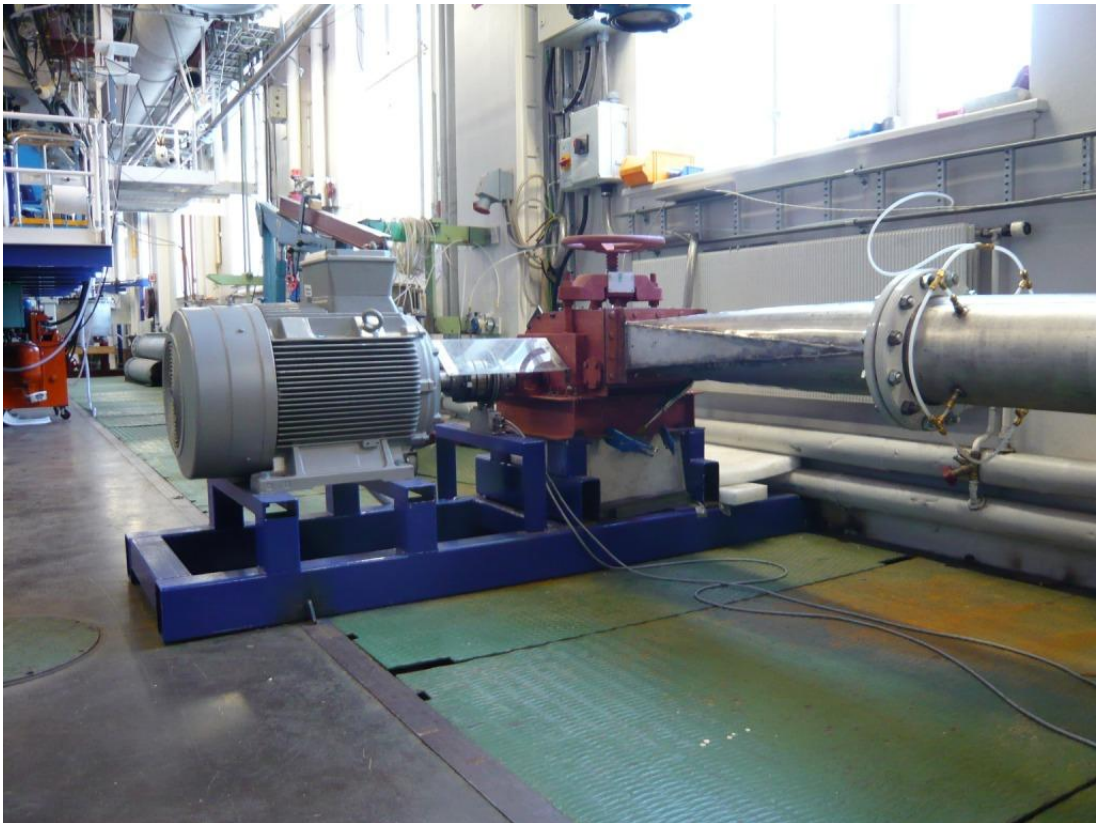
Pictures of the experimental setup

Figure L.1: The cross–flow turbine and generator

Figure L.2: The cross–flow turbine after remodeling